TOPICAL REVIEW • OPEN ACCESS

Recent progress in two dimensional Mxenes for photocatalysis: a critical review

To cite this article: Tahir Haneef *et al* 2023 *2D Mater.* **10** 012001

2D Materials

TOPICAL REVIEW

Recent progress in two dimensional Mxenes for photocatalysis: a critical review

Tahir Haneef[1], Kashif Rasool[2,*], Jibran Iqbal[3], Rab Nawaz[4], Muhammad Raza Ul Mustafa[5,6], Khaled A Mahmoud[2], Tapati Sarkar[7] and Asif Shahzad[7,*]

[1] Civil and Environmental Engineering Department, The University of Alabama in Huntsville, Huntsville, AL 35899, United States of America
[2] Qatar Environment and Energy Research Institute (QEERI), Hamad Bin Khalifa University (HBKU), PO Box 5825, Doha, Qatar
[3] College of Natural and Health Sciences, Zayed University, Abu Dhabi 144534, United Arab Emirates
[4] Fundamental and Applied Sciences Department (FASD), Universiti Teknologi PETRONAS, Bandar Seri Iskandar 32610, Perak, Malaysia
[5] Department of Civil and Environmental Engineering, Universiti Teknologi PETRONAS, Seri Iskandar 32610, Perak, Malaysia
[6] Centre for Urban Resource Sustainability, Institute of Self-Sustainable Building, Universiti Teknologi PETRONAS, Seri Iskandar 32610, Perak, Malaysia
[7] Department of Materials Science and Engineering, Uppsala University, Box 35, SE-75103 Uppsala, Sweden
* Authors to whom any correspondence should be addressed.

E-mail: krasool@hbku.edu.qa and asifshzd8@gmail.com

Keywords: transition metal carbide, 2D MXenes, photocatalysis, hydrogen evolution, carbon dioxide reduction, organic pollutants, wastewater treatment

OPEN ACCESS

RECEIVED
12 May 2022

REVISED
7 September 2022

ACCEPTED FOR PUBLICATION
28 October 2022

PUBLISHED
18 November 2022

Abstract

Transition metal carbides and nitrides, generally known as MXenes have emerged as an alternative to improve photocatalytic performance in renewable energy and environmental remediation applications because of their high surface area, tunable chemistry, and easily adjustable elemental compositions. MXenes have many interlayer groups, surface group operations, and a flexible layer spacing that makes them ideal catalysts. Over 30 different members of the MXenes family have been explored and successfully utilized as catalysts. Particularly, MXenes have achieved success as a photocatalyst for carbon dioxide reduction, nitrogen fixation, hydrogen evolution, and photochemical degradation. The structure of MXenes and the presence of hydrophilic functional groups on the surface results in excellent photocatalytic hydrogen evolution. In addition, MXenes' surface defects provide abundant CO_2 adsorption sites. Moreover, their highly efficient catalytic oxidation activity is a result of their excellent two-dimensional nanomaterial structure and high-speed electron transport channels. This article comprehensively discusses the structure, synthesis techniques, photocatalytic applications (i.e. H_2 evolution, N_2 fixation, CO_2 reduction, and degradation of pollutants), and recyclability of MXenes. This review also critically evaluates the MXene-based heterostructure and composites photocatalyst synthesis process and their performance for organic pollutant degradation. Finally, a prospect for further research is presented in environmental and energy sciences.

1. Introduction

Currently, there is a great focus on developing efficient, stable, and recyclable semiconductor catalysts to counter energy shortage, global warming, and environmental pollution challenges [1, 2]. There have been many semiconductor catalysts discovered over the past few decades, such as TiO_2 [3], ZnO [4], Fe_2O_3 [2], graphitic carbon nitride (g-C_3N_4) [5], and BiOX (X = Cl, Br) [6]. The photocatalysts are used for the conversion of CO_2 into hydrocarbon fuel, the photocatalytic evolution of hydrogen, and the degradation of pollutants. The photocatalytic activity of these materials is not adequate to make them suitable for industrial applications due to the weak absorption of visible light in semiconductor materials, the rapid recombination rate of photogenerated electron–hole pairs, lack of active sites, inability to regenerate, and instability [7–10]. As a result, a great deal of effort has gone into improving the

photocatalytic activity and other desired properties of semiconductor catalysts. These efforts include element doping, surface sensitization, facet control, and assembly of heterojunctions [11]. In many different strategies, heterostructure photocatalyst designs have been developed to improve the separation efficiency of photogenerated charge carriers [12].

Two-dimensional (2D) frameworks have received much attention since the discovery of monolayered graphene in 2004 [13]. Since then, 2D materials exhibiting excellent catalytic, optoelectronic, and electronic properties have been developed, such as black phosphorous [14], layered double hydroxides (LDHs) [15], transition metal chalcogenides, etc [16]. 2D materials enhance photocatalytic activity because their structure prevents charge carriers from recombination. MXene, first developed in 2011, is one of the most interesting classes of 2D nanomaterials and has been proposed for numerous applications including energy production [17–22], magnetic shielding effects [23–26], energy storage batteries [27–32] and capacitors [33–36], medical and biomedical applications [37–42], water splitting [43–47] and water/wastewater purification [1, 48–50]. In water purification, MXenes are being used in membrane fabrication, adsorption, and photocatalysis of organic contaminants [51–55]. The following factors account for the successful applications of MXenes in photocatalysis: (a) wet chemical etching results in surface functional group formation that make MXene surfaces negatively charged and results in the formation of stable dispersions [56]. (b) Tuning the surface chemistry of MXene can influence the bandgap alignment [57]. (c) Because of their conductive metal cores, MXenes have high metallic conductivity and great electron acceptance abilities [58, 59]. Therefore, MXenes are considered a potential addition to 2D engineering materials and are being widely investigated for a variety of photocatalytic applications. Using MXene as an enhancement material, it might be possible to promote charge carrier separation, function as robust support, limit the size of photocatalysts or enhance reactant adsorption in these applications [11, 60]. As a substrate, MXenes could host either one or more catalysts to achieve higher photocatalytic activity [61]. Furthermore, Schottky barriers form between MXenes and semiconductor catalysts that could inhibit the recombination of charge carriers during photocatalysis [52, 62]. Additionally, the large specific surface area of MXenes provides many active sites for photocatalysis [11, 63, 64].

Owing to the unique properties of MXenes, there is a rapid growth in research on the synthesis and use of MXenes and MXene-based nanomaterials for photocatalytic applications. Up to now, titanium carbide MXene ($Ti_3C_2T_x$) is the most studied MXene member and hence many recent articles have reviewed Ti_3C_2 MXene's potential for energy conversion and storage applications including supercapacitors and batteries, however, a few have focused on its use in photocatalytic applications [46, 59, 63, 65–68]. In 2021, Liqun *et al* reviewed the photocatalytic application of MXene [55, 69]. However, the author only focused on one member of the MXene family, Ti_3C_2. Moreover, the review is short and does not cover all the work published on the concentrated topic, and lacks critical analysis. To develop an innovative future framework, we believe it is necessary to carefully review, discuss, and analyze all the published work in this field. To our knowledge, no comprehensive review has been published covering the structure, synthesis, photocatalytic applications, and recyclability of MXenes. It is imperative to conduct a literature review that describes synthesis techniques and photocatalytic applications of MXenes along with their structure and reusability. Presenting the latest studies and developments in this important field along with challenges and recommendations will surely increase the attention of the scientific community. Thus, in this review, we have focused on the structure, synthesis, and photocatalytic applications of MXenes. Hydrogen (H_2) evolution, nitrogen (N_2) fixation, carbon dioxide (CO_2) reduction, degradation of organic/inorganic pollutants, and recyclability of MXenes have been explored and discussed in detail. Finally, the challenges and future perspectives in research in MXenes have been discussed in this review.

2. Structure of MXenes

MXenes are new emerging 2D materials composed of transition metal carbides and nitrides exfoliated from MAX phases ($M_{n+1}AX_n$) (M = Mo, Ti, Zr, Cr, A = Al, Ga, Ge, Si, and X = C, N); the structure as well as the composition of MXenes depend on the MAX phases. Generally, MAX phases can be classified into various types based on the initial stoichiometric ratio of selected elements such as 211, 312, 413 etc depending on the value of n in the MAX phase which usually ranges between 1 and 3. The first MXenes, $Ti_3C_2T_x$, exfoliated from the Ti_3AlC_2 (312) MAX phase was reported by Naguib *et al* [70, 71]. MXenes have exhibited tremendous structural properties which could make them an excellent potential classe of 2D materials in the field of photocatalysis. The following properties of MXenes could play important roles in photocatalysis: (a) 2D MXenes have a large surface area, which boosts catalytic activity and flexibility of the catalyst. (b) Planar structures of 2D MXenes provide abundant surface atoms and enough space for compounding with semiconductor photocatalysts. (c) The main structural feature of 2D MXenes is that its thickness is extremely low.

MXenes have a hexagonal structure like the ternary nitrides and carbides phase (MAX phase) since they are derived by etching the A atoms of their precursor material. MXene crystals have a hexagonally close-packed (HCP) structure. It has

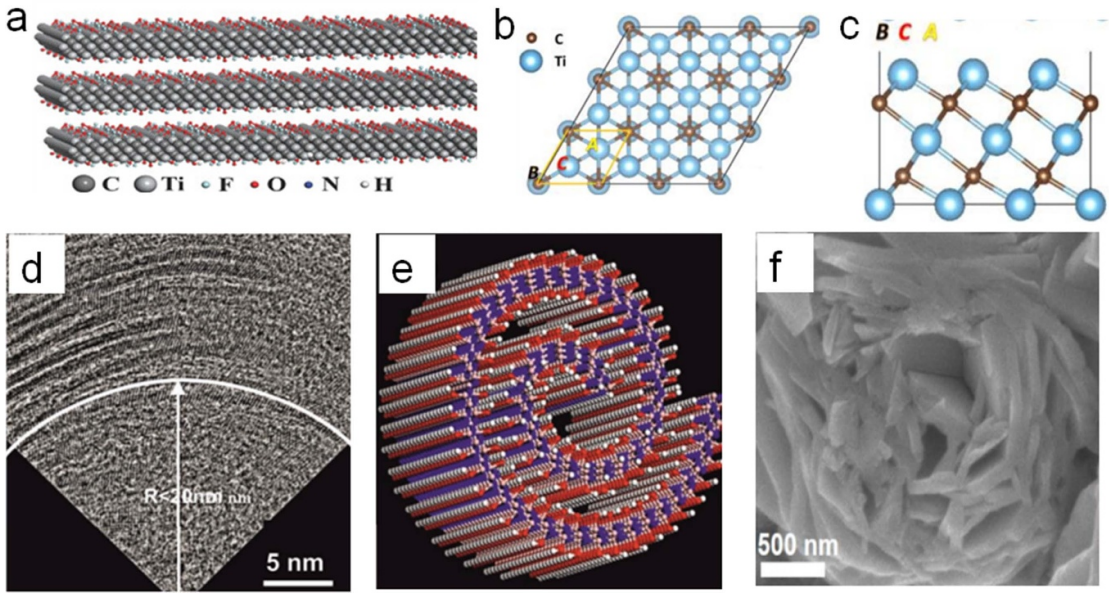

Figure 1. (a) Schematic diagram showing the crystal structure of a Ti_3C_2 monolayer ([76] John Wiley & Sons. © 2017 WILEY-VCH Verlag GmbH & Co. KGaA, Weinheim) (b) top and (c) side view. Reprinted with permission from [77]. Copyright (2014) American Chemical Society. Schematic illustration of MXenes' Structure (d) TEM image of Ti_3C_2 nanoscroll and (e) schematic of the MXene nanoscroll. [70] John Wiley & Sons. Copyright © 2011 WILEY-VCH Verlag GmbH & Co. KGaA, Weinheim. (f) SEM image of flower-like $Ti_3C_2T_x$. Reprinted with permission from [82]. Copyright (2019) American Chemical Society.

been noted that M_2X MXenes exhibit an HCP sequence (ABABAB), while M_3X_2 and M_4X_3 have a face centered cubic (FCC) sequence (ABCABC) [71]. An atomic arrangement like this is important when synthesizing MXenes that involve M elements with HCP ordering in bulk states. For instance, a recent density functional theory (DFT) calculation has revealed greater stability for hexagonal molybdenum carbides ($Mo_3C_2T_x$ or $Mo_4C_3T_x$) compared with their FCC counterparts [72, 73]. Furthermore, based on the formation energies of MXenes, it is found that $Mo_3C_2T_x$ and $Mo_4C_3T_x$ are unstable because their M atoms are arranged like those of rock salt; however, Mo_2CT_x is stable. The unstable Mo-C bonds are prevented by inserting another transition metal, Ti, into the structure, which bonds with C and prevents them from becoming unstable. By doing so, a collection of ordered double-M element 2D carbides are formed, such as $(Mo_2Ti)C_2T_x$ and $(MoTi_2)C_3T_x$ [74, 75]. In addition, figures 1(a)–(c) shows the three different parts of the structure of $Ti_3C_2T_x$: the interlayer skeleton, the interlayer structure, and the surface terminating groups [69, 76, 77]. An intramolecular skeleton is formed when Ti atoms are stacked with C atoms alternately to create ionic bonds, which is the basis for the entire main structure [78]. Neutron diffraction studies completed on the interlayer region demonstrated that the interaction between the layers is developed by hydrogen bonds between either the F or O atoms on the surface, as well as van der Waals forces between the atoms [79]. It is not only the orientation of –OH in the sheet that affects the strength of the interlayer hydrogen bonding, but also the number and distribution of –OH groups. Whenever water molecule occurs between layers, it is also capable of hydrogen bonding. Additionally, the $Ti_3C_2T_x$ main structure is covered by a large number of randomly distributed terminal groups [69]. The characteristics of the $Ti_3C_2T_x$ produced are greatly influenced by the surface groups, which may be studied using electron energy loss spectroscopy (TEM), neutron scattering, and nuclear magnetic resonance spectroscopy (NMR) methods [80, 81]. MXene terminations are generally randomly distributed and mixed, which depends majorly on the synthesized conditions, transition metal elements, and post-synthesis treatments [7].

As far as their morphology is concerned, most MXenes exhibit accordion-like multilayer structures. Nevertheless, MXenes with different structures have also been synthesized [7]. As shown in figures 1(d) and (e), Naguib *et al* [70] produced scroll-like $Ti_3C_2T_x$ with radii less than 20 nm by using sonication for exfoliation. Additionally, the ethanediamine-treated flower-like $Ti_3C_2T_x$ was prepared by hydrothermal treatment for 8 h at 80 °C (figure 1(f)) [82]. The presence of MXene nanofibers and nanoribbons has been observed in some cases [7].

3. Synthesis of MXenes

MXenes are emerging 2D nanomaterials derived from MAX phases ($M_{n+1}AX_n$) which are ternary nitrides and carbides [83]. A MAX phase can be fabricated by combining an element from early d-block transition

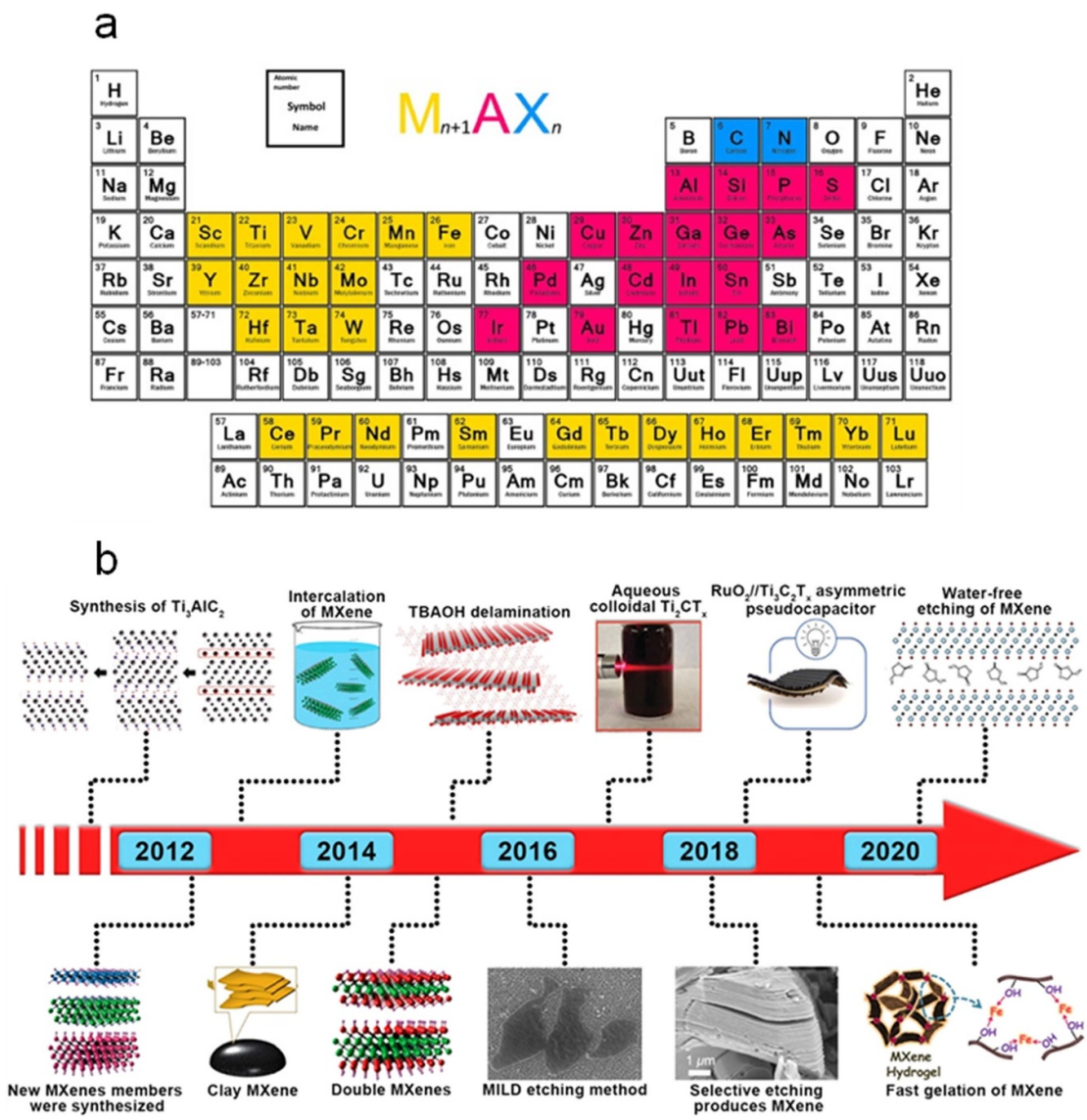

Figure 2. (a) Elements known to form MAX Phases. Reprinted from [84], Copyright (2019), with permission from Elsevier. (b) Schematic of the progress in MXene synthesis over the first 10 years. Reprinted from [87], Copyright (2021), with permission from Elsevier.

metals such as Ti (M) group A element (Al) and C or N (X) (figure 2(a)) [84]. 211 (M_2AX), 312 (M_3AX_2), and 413 (M_4AX_3) MAX phases can be synthesized by changing the initial concentration of the elements and synthesis protocols. MXenes are generally synthesized by etching the A layer from the above mentioned MAX phases by an etching process [55, 73]. MXenes can be further categorized into three kinds based on the initial stoichiometric ratio of the selected elements: (a) The most common form of MXene is a mono-M element containing one transition metal. (b) Solid-solution M elements MXenes constitue a second of MXenes, which contain two different configurations of transition metals in the same layer [85]. (c) A third type of MXenes is the sordered double-M elements M'M"Xene. Just M_3X_2 and M_4X_3 are examples of double-M elements M'M"Xene [73, 86].

In comparison to the M–X bonds, the M–A bonds are generally weaker and more reactive, therefore the MXenes are fabricated after removing A-elements from the MAX phases [88]. In contrast to the van der Waals interaction found in layered materials such as graphite and transition metal dichalcogenides, the metal bond created between the $M_{n+1}X_n$ layers is much stronger [46]. The higher strength and rigidity of MXenes are advantageous to their long-term performance for photocatalytic applications. In 2011, Naguib *et al* [70], synthesized the first MXene by etching Ti_3AlC_2 with hydrofluoric acid (HF), while up to now several MXenes have been synthesized via different advanced techniques as shown in figure 2(b) [87]. By wet-chemical etching MAX phases, these subsequent MXenes are formed. The most common methods of etching include HF etching, fluoride etching, and a few others. The synthesis methods of

Table 1. Different synthesis methods of MXene and applications.

Materials	Method	Application	Efficiency %	References
MXene/$NiFe_2O_4$	One-step hydrothermal method	Microwave absorption	40	[89]
Nickel-cobalt layered double hydroxide/MXene	Heterojunction surface	Photocatalytic bactericidal	—	[90]
$Ti_3C_2T_x$ MXene nanosheets	Controlled oxidation action	MXsorption of mercury	90	[91]
Ti_2CT_x MXene	3D spheroid-type cultures	Biocompatibility and biophysical	98	[92]
$Ti_3C_2T_z$ MXene	Intensive layer delamination and acid etching	Inexpensive precursor material	—	[93]
Cr_2CT_x MXene	Etching	Hydrogen evolution reaction	85	[94]
TiO_2@Ti_3C_2 nanoflowers MXene	*In situ* Transformation	Photocatalytic activity	97	[95]
Mo_2CT_x MXene	Mo_2Ga_2C by etching	Thermal stability	—	[96]

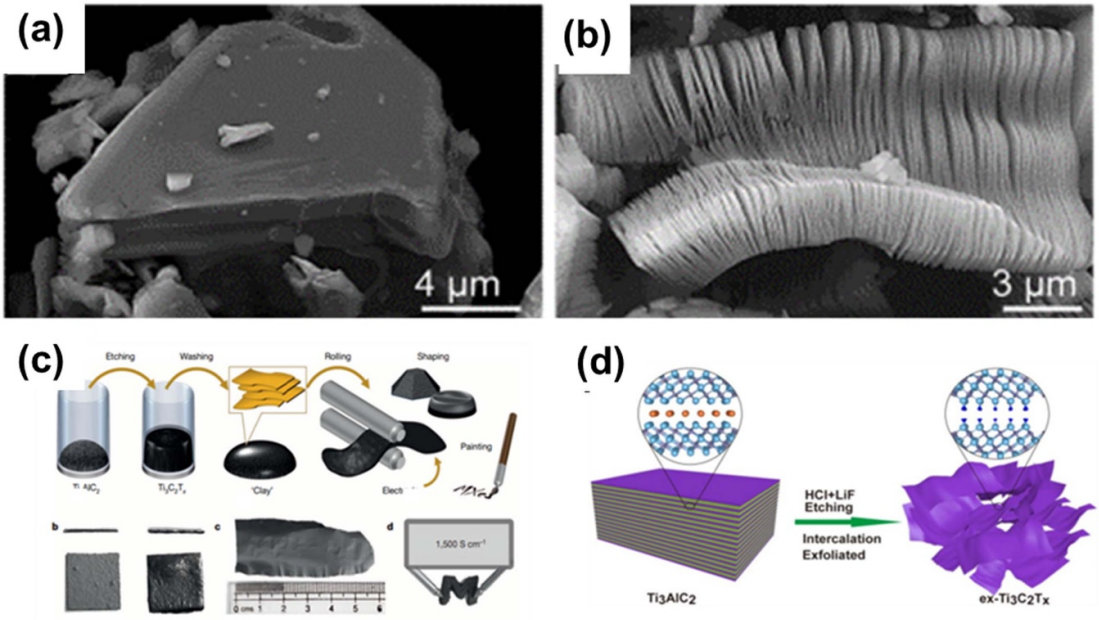

Figure 3. HF etching methods used to obtain MXenes: (a) FESEM image of untreated Ti_3AlC_2 MAX phase and (b) SEM image of $Ti_3C_2T_x$ after HF treatment, Floride etching methods used to obtain MXenes. (a), (b) Reprinted from [100], © 2020 Elsevier Ltd and Techna Group S.r.l. All rights reserved. (c) Schematic of synthesis of MXene clay and electrode. (d) Schematic illustration for the preparation of MXene via HCl/fluorides etching, intercalation, and exfoliation under H_2O sonication. (c), (d) Reprinted with permission from [110]. Copyright (2019) American Chemical Society.

MXenes may affect their efficiency in various applications as shown in table 1.

3.1. MAX phase etching by hydrofluoric acid

Most MAX phases can be etched with hydrofluoric acid at various temperatures to produce different MXenes, depending on the different HF parameters such as concentration and environmental conditions like room temperature (figures 3(a)–(d)) table 2 [70, 84, 97–100]. HF has very high selectivity as an etchant, allowing it to selectively remove distinct kinds of SiC [101]. The etching conditions for the MAX phase containing Al vary based on different factors such as particle size, atomic bond, and structure of transition metal [102]. As an example, in the most commonly investigated $Ti_3C_2T_X$, 0.5 g Ti_3AlC_2 MAX phase is progressively introduced to 10 ml etchant and agitated with a Teflon magnetic bar at room temperature [103]. The slow addition of Ti_3AlC_2 MAX is preferred, to inhibit the formation of excessive bubbles during the exothermic reaction. Hydrogen bonds and van der Waals bonds keep the layers of the fabricated MXene powders (2-dimensional) together [104]. However,

Table 2. Different parameters of HF etching.

MXene type	Synthesis method	Concentration	Time (h)	Temperature °C	References
$Ti_3C_2T_x$ MXene	HF etching	48%	24	45	[112]
Ti_3C_2 MXene	HF etching	49%	2	40	[113]
2D Molybdenum Carbide	HF etching	14 M	158.4	55	[114]
$Ti_3C_2T_x$ MXene	HF etching	50%	90	55	[115]
Conductive two-dimensional titanium carbide	HF etching	50%	24	35	[116]
$Ti_3C_2T_x$ MXene	HFetching	49.5%	18	23	[104]

it is important to recognize that using high concentrations of HF as an etchant can cause a lot of defects in the $Ti_3C_2T_X$ nanosheets, and a prolonged etching period can also damage the MXene's layered structure [105, 106]. The following model equations can be used to illustrate the fabrication of MXenes [83, 107]:

$$3HF + M_{n+1}AX_n \rightarrow M_{n+1}X_n + AF_3 + 3/2\ H_2 \quad (1)$$

$$2H_2O + M_{n+1}X_n \rightarrow H_2 + M_{n+1}X_n(OH)_2 \quad (2)$$

$$2HF + M_{n+1}X_n \rightarrow H_2 + M_{n+1}X_nF_2. \quad (3)$$

In the first stage, the MXene layers are formed after the reaction of A layers of MAX phases with HF or fluoride ions, while in the second stage the MAX phases' A atoms are substituted with –OH, –O, and/or –F groups. During the third stage reaction, the interaction between the $M_{n+1}X_n$ layers becomes weak causing loosely packed, graphite-like layered structures to form. In the presence of surface functional groups (–OH, –O, and/or –F), MXene surfaces become negatively charged, resulting in the formation of stable dispersions (flake sizes range from 1 to 10 μm) [83]. Several novel MXenes, including Mo_2C, Ti_2C, and Ti_3SiC_2, have been prepared using the HF etching method [108]. Furthermore, because HF is a very corrosive acid, its extensive use as an etchant is not only hazardous for, humans but also pollutes the environment. Moreover, this process cannot synthesize stable MXenes ($Ti_{n+1}N_n$) based on nitride-based metals [109]. Therefore, it is necessary to develop environmentally friendly and more versatile protocols for MXene synthesis.

HF is highly toxic, reactive, and corrosive, therefore, it is hazardous for regular use in the lab, and hence, its direct use should be avoided. As an alternative to the direct use of HF, MXenes can be produced by an etching agent prepared by combining fluoride salts (such as MF and FeF_3) and strong acids (H_2SO_4 and HCl) [109]. Fluoride salts react *in situ* with the strong acids to produce hydrogen fluoride through the process of etching, the strong acids provide the H^+ and the fluoride salts release the F^-. In the meantime, cations and water molecules can intercalate into MXenes, increasing interlayer distance and weakening interlayer contact, resulting in material delamination during sonication [117]. Hence, this approach simplifies the process that involves the use of concentrated HF and a time-consuming multi-step procedure, allowing a one-step synthesis of MXenes. Yin's group has developed $Ti_3C_2T_x$ by etching, intercalating, and exfoliating Ti_3AlC_2 powder with HCl/fluorides in water under ultrasonication as shown in figure 3(e) [110]. Similarly, Ghidiu *et al* [116], effectively produced $Ti_3C_2T_x$ clay using an HCl/LiF combination as the etching agent. During the etching process, LiF interacts with HCl (equation (4)) to generate HF, and the quantity of HF may be precisely controlled without harming the $Ti_3C_2T_x$ structure. In comparison with pure HF, the LiF and HCl mixture performed better as an etchant, and the produced Ti_3C_2 exhibited no nanoscale defects [116, 118]. Monolayered or multilayered MXenes can be obtained immediately by washing away the reaction products, as *in situ* produced HF etches the Ti_3AlC_2 [119]. Notably, a clay-like paste obtained from this process can be repeatedly rolled into flexible and free-standing films, showing the material has good flexibility and strength as shown in figure 3(f) [111]. Likewise, MXenes like Ti_2C [120], Ti_3CN [121, 122], Cr_2TiC_2 [122], and $(Nb_{0.8}Zr_{0.2})_4C_3$ [30] were also synthesized by etching other MAX phases with LiF and HCl mixed solution:

$$HCl + LiF \rightarrow HF + LiCl. \quad (4)$$

In addition, a combination of various fluoride salts such as MF, FeF_3, CaF_2, and acids might also be used as etchants to synthesize MXenes. Furthermore, difluorides such as KHF_2 or NH_4HF_2 are viable etchants for Ti_3AlC_2. In Ti_3AlC_2, both etching, and intercalation of cations take place concurrently, and the cations can enhance $Ti_3C_2T_x$ interplanar space, maintaining the 2D flake structure of the material [104]. As reported in related publications, MXenes can also be synthesized by etching MAX phases using a hydrothermal process. Peng *et al* [123] reported the preparation of two types of 2D MXenes (Nb_2C and Ti_3C) without the direct use of HF, and using instead, $NaBF_4$ and HCl hydrothermal etching as a method of preparation. In the hydrothermal environment,

$NaBF_4$ interacts with HCl to produce HF *in situ*. The MAX phase is then etched with HF as a fluorine source, generating the corresponding MXenes, namely $Ti_3C_2T_x$ and Nb_2C [87, 123]. Comparing fluoride etching with HF etching, fluoride etching exhibits more advantages, such as bigger flakes, fewer defects, higher interlayer spacing due to cation intercalation, and simpler operation. As an additional benefit, the sonication treatment can directly create single layers or a few layers of MXenes without using any organic molecular reagent [124]. In contrast with MXenes obtained by HF etching, this method is unable to produce the accordion-like morphology of MXenes, which require higher etching temperatures and longer etching times. Furthermore, the etching process is dynamic, and the conditions for conversion for different kinds of MXenes may vary.

3.2. MAX phase etching by other methods

Besides etching methods using HF and fluoride salts, several new etching techniques for MXene manufacturing have recently been discovered [125]. In a recent report, Li *et al* [126], described a typical alkali-hydrothermal method for the preparation of $Ti_3C_2T_z$ (T = OH, –O) MXene (figure 4(a) [103]). This approach is based on the Bayer process, which is widely utilized in the bauxite refining industry. The entire process is fluorine-free, and multilayer $Ti_3C_2T_z$ with a purity of approximately 92% (via 27.5 M NaOH, 270 °C) was formed. It was the first time that an alkali etching method was used to synthesize high-purity multilayer MXenes [126]. The hydrothermally fabricated $Ti_3C_2T_x$ has a larger interlayer distance and a higher specific surface area than $Ti_3C_2T_x$ synthesized through conventional HF etching, because of the hydrothermal slow-release mechanism. Since the hydrothermal etching method avoids the need for high consistency HF, it is also more effective for synthesizing $Ti_3C_2T_x$ thin films [127].

The electrochemical etching technique has been shown to have a promising etching impact on MAX precursors, allowing for the selective removal of layer nano components. Sun *et al* [128], proved an effective electrochemical etching route for preparing $Ti_3C_2T_x$ MXene. A layer of $Ti_3C_2T_x$ MXene on Ti_2Al was formed after electrochemically etching Al from porous Ti_2AlC in diluted hydrochloride acid (figure 4(b)). The MXenes only contain –Cl terminal groups, along with the more common –O and –OH groups. Furthermore, the electrochemical etching process can also over-etch the parent MAX phases into carbide-derived carbons (CDC). To produce MXenes without over-etching, a careful balance is required in the etching parameters [128]. In addition, electrochemical etching products are hydrophilic in absence of fluorine terminations due to the HF-free etching. This method overcomes the etching energy barrier, gives a flexible range of etching conditions, and allows a variety of etchants to be used. The electrochemical etching method offers a more environmentally friendly route for the production of 2D MXenes with an accurately controllable surface [127, 129]. The introduction of an electrochemical etching technique using diluted hydrochloric acid to produce MXenes provides a viable solution to the long-standing problem of excessive HF concentration. Nevertheless, for large-scale production to be successful, issues about low yield need to be resolved.

In a recent study, for the first time, researchers reported a new route of MXene synthesis via the Lewis acidic etching system [130, 131]. The Ti_3SiC phase was immersed in Cu Lewis molten salt at 750°C (figure 4(c)) [132]. $Ti_3C_2Cl_2$ MXene in powdered form was obtained after the chemical reaction between Ti_3SiC_2 and $CuCl_2$. Then $Ti_3C_2Cl_2$ was further washed with ammonium persulfate ($(NH_4)_2S_2O_8$) to obtain the final product MS-$Ti_3C_2Cl_2$ (molten salt-MXene) [131]. The chloride ion plays a crucial role in Lewis acidic etching as it does in electrochemical etching. This technique can potentially be used with any Lewis acid salt with a greater redox potential than the corresponding A element [133]. Lewis acidic etching system enables the fabrication of new 2D materials that are impossible or extremely difficult to obtain via conventional synthesis methods. This method broadens the variety of MAX-phase precursors that may be employed, and it opens up new possibilities for fine-tuning the surface chemistry and characteristics of MXenes [134].

MAX etching is also reported using halogen as an etchant. In Shi *et al*'s work, the authors used I_2 to etch Ti_3AlC_2 at 100°C with anhydrous acetonitrile, resulting in $Ti_3C_2I_x$ that resembles an accordion-like structure [135]. A solution of 1 M HCl was applied afterward to remove any residual AlI_3 formed during the etching process. In the HCl solution, -I groups are transformed to –OH and –O due to the instability of the surface groups. This method enabled the production of fluorine-free $Ti_3C_2T_x$ (T = O, OH). The recent research of Jawaid and colleagues reported that Ti_3AlC_2 was etched in organic solvents containing halogens and interhalogens, providing homogeneous Cl, Br, or I terminations on synthesized MXenes (figure 4(d)) [136]. The halogen groups on the surface were not converted as the etching process was conducted inside a glove box and the final products were stored in tetrahydrofuran solvent [134].

3.3. Delamination of MXenes

The synthesized MXene is produced in multilayers and delamination is required to produce MXene sheets with just one or a few layers. In the etching process, hydrogen bonds and van der Waals forces substitute the strong M–A bonds, so multi-layer MXenes can be layered by adding intercalators. Despite this, MXenes exhibit much stronger interlaminar interactions than graphite, it still has approximately 2–6

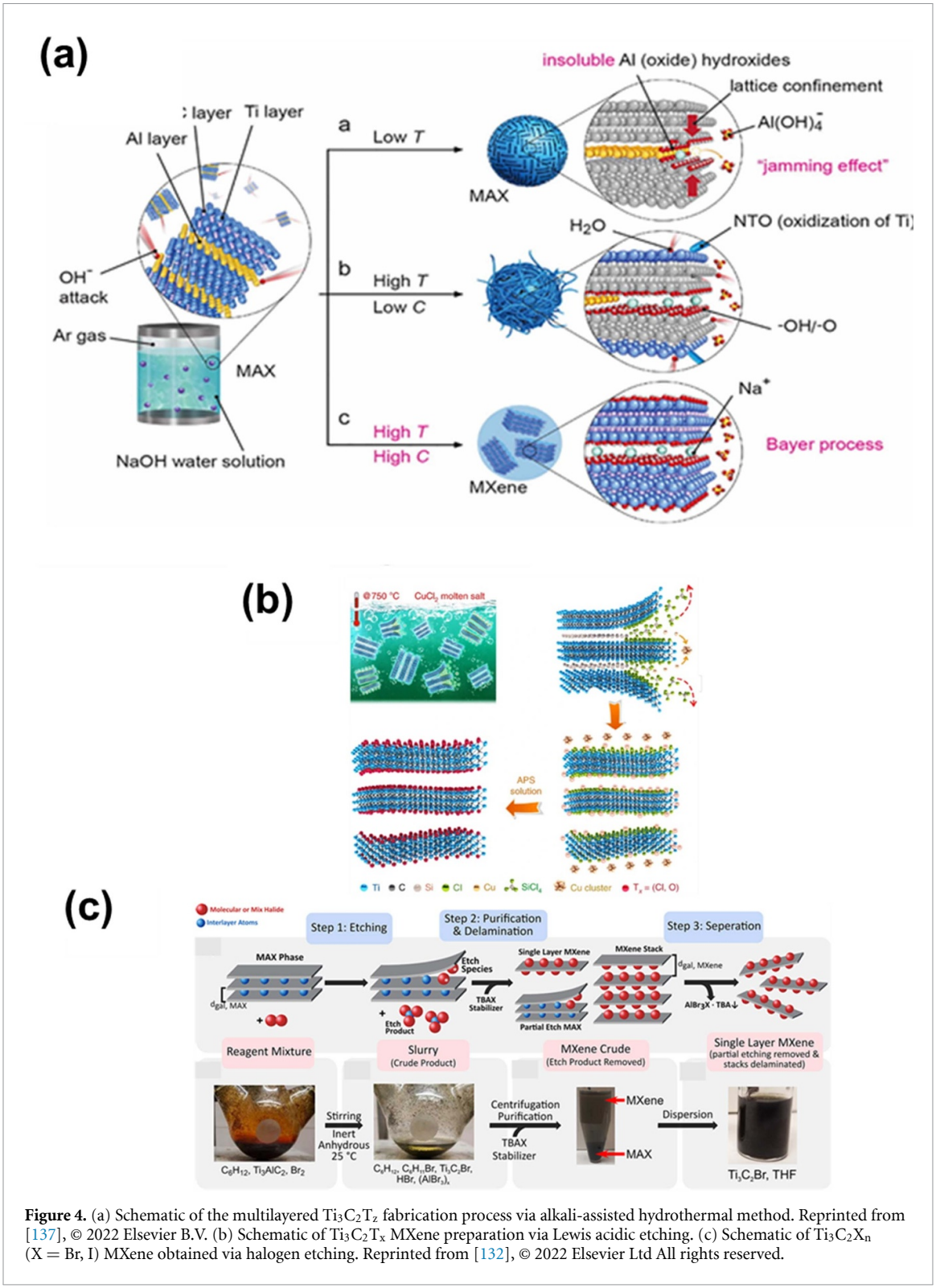

Figure 4. (a) Schematic of the multilayered $Ti_3C_2T_z$ fabrication process via alkali-assisted hydrothermal method. Reprinted from [137], © 2022 Elsevier B.V. (b) Schematic of $Ti_3C_2T_x$ MXene preparation via Lewis acidic etching. (c) Schematic of $Ti_3C_2X_n$ (X = Br, I) MXene obtained via halogen etching. Reprinted from [132], © 2022 Elsevier Ltd All rights reserved.

times the strength of graphite [138, 139]. Therefore, the transparent tape method cannot form a single layer of MXene by mechanical peeling. A common method of delaminating MXenes is to intercalate the material before mechanical stirring. The interlayer spacing of $Ti_3C_2T_z$ flakes can be widened using intercalation compounds, which results in weaker interactions between the 2D layers [140, 141]. An appropriate solvent for the intercalating agent and material should be carefully chosen during the intercalation and delamination processes. Two steps are involved in introducing the intercalator into the 2D sheet. Using the ultrasonic treatment and centrifugation steps combined in this step, it is possible to separate the layered material from the multilayer (nonlayered). The desired sheet size and density determine the ultrasonic processing stage. The resulting colloidal solution will comprise scattered 2D

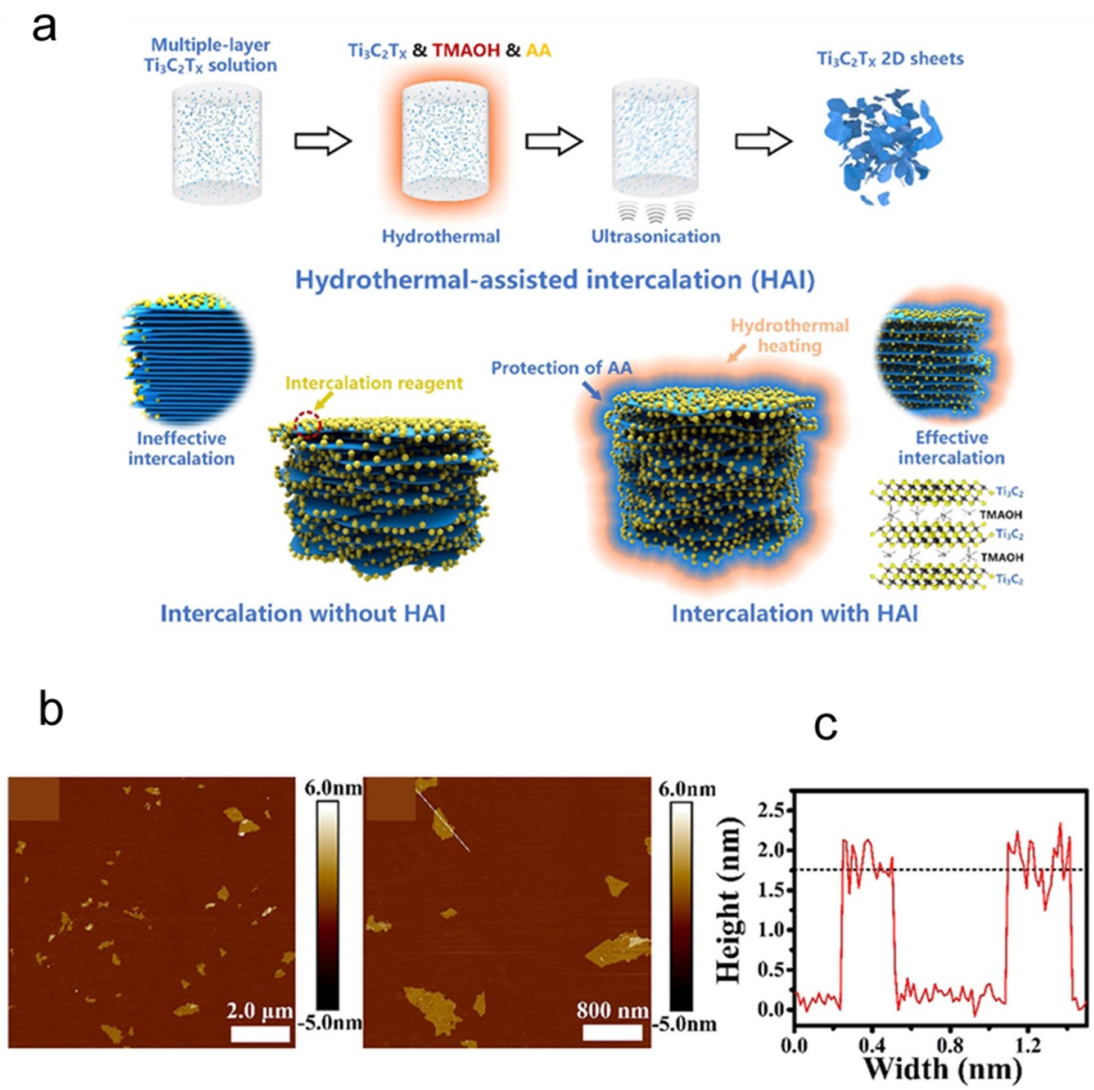

Figure 5. Schematic demonstration and illustration of delamination. (a) The designed HAI strategy to synthesize $Ti_3C_2T_x$ 2D sheets. (b) AFM images and (c) height profile. (a)–(c) Reprinted with permission from [145]. Copyright (2019) American Chemical Society.

sheets of electrostatically stabilized MXenes that are processable and functional, as well as stable against aggregation or clumping [142]. Furthermore, the steps of ultrasonic processing are adapted according to the type of etching techniques used and the application requirements. To produce smaller flakes with more flaws, it is necessary to increase the ultrasonic power and duration of the ultrasonic process. MXene concentration in the solution is also affected by the technique and type of intercalator that is used during synthesis [87, 143]. Even though ultrasonic treatment was utilized to delaminate the few-layer thick MXenes in initial reports, the delaminated layers had a low yield because MXenes interact strongly with each other. Therefore, it is crucial to break the prevailing interlayer forces to separate the stacked nanosheets of MXenes. It has proven feasible to weaken interlayer interactions and increase the interlayer spacing between these layers by injecting organic molecules or inorganic ions into them [134].

Various organic solvents such as dimethyl sulfoxide (DMSO), hydrazine monohydrate (HM), and N,N-dimethylformamide (DMF), have been used as intercalates for multilayer MXene exfoliation [142]. Even though DMSO exhibited promising results when used as an agent for intercalation of $Ti_3C_2T_x$, it does not affect the intercalation of other MXenes, such as V_2CT_x or Mo_2CT_x. In contrast with DMSO, the organic bases with relatively large molecule tetrabutylammonium hydroxide (TBAOH), hydroxyl choline, and n-butylamine, exhibit universal intercalating nature [144]. Han *et al* [145] reported that the bond interaction between the Ti-Ti and Ti-Al inside the $Ti_3C_2T_x$ layers are the main impediments besides the van der Waals forces. In a hydrothermal process, TMAOH is diffused and intercalated into multilayer MXenes, resulting in their subsequent delamination figure 5(a). Ascorbic acid was utilized as a moderate reductant to prevent MXenes from oxidizing at high temperatures. Figure 5(b) shows the AFM image

of bilayered 2D $Ti_3C_2T_x$ nanosheets with a thickness of 1.7 nm (figure 5(c)), which confirmed the successful fabrication [145]. Furthermore, the TMAOH could intercalate and delaminate the MXene with the help of microwaves, although the yield of monolayer MXene nanosheets was relatively low, limiting its preparative applications [146, 147]. Since TMAOH is one of the main ingredients in commercial etchants for Al. Xuan *et al* reported that the high reactivity between TMAOH and Al atoms made TMAOH a suitable etchant and intercalator for synthesizing monolayers of $Ti_3C_2T_x$ from Ti_3AlC_2, where other organic intercalators (DMSO, urea, and hydrazine) were not effective [134, 148]. Currently, delamination of multilayer MXenes is typically performed on products generated by HF etching or other aqueous etching processes. Therefore, further exploration is needed to determine how organic intercalators can be used in non-aqueous systems.

4. Photocatalytic applications of MXenes

4.1. Basic principle of photocatalysis

Photoelectrochemical devices were introduced by Fujishima and Honda in 1972, which decompose water into oxygen and hydrogen when exposed to visible light. Furthermore, they claimed that water splitting could take place regardless of the voltage applied, as long as certain conditions were met [149]. In general, photocatalytic reactions can be broken down into the following five main steps (a) light absorption, (b) charge separation, (c) charge migration, (d) interfacial charge transfer, and (e) surface reaction [150]. The efficiency of photocatalysis can be influenced by each of these stages. To improve and optimize the photocatalytic reaction, each factor needs to be tuned for practical application. In an aqueous solution, three major active groups participate in the photocatalytic reaction: OH (hydroxyl radical), h^+ (hole), and $\cdot O^-_2$ (superoxide radical), where OH is the main oxidant [151]. There is a notable fact that electrons can only be excited from the valence band (VB) to the conduction band (CB) as long as the energy of the incident photons ($h\nu$) exceeds or equals the bandgap (E_g) of the photocatalyst. A negatively charged high-reactive electron (e^-) is generated in the CB, leaving an electropositive hole (h^+) in the VB, thus resulting in the photoexcited electrons and holes. The incident light's wavelength must fulfill the following criteria [7]:

$$\lambda \leqslant ch/Eg. \tag{5}$$

In the equation, c stands for velocity of light, λ for wavelength, and h for Planck's constant, while E_g denotes the semiconductor bandgap.

TiO_2 and ZnO are the most commonly used photocatalysts, however, their wide band gaps make them less effective in sunlight. Only 9.3% of the solar light consists of ultraviolet light, which can generate electron–hole pairs in these semiconductors. Many advances were made toward the synthesis of visible-light-active TiO_2 and ZnO utilizing various approaches, including surface alteration and bandgap generation [67]. Currently, many studies are being carried out using semiconductors having bandgaps suitable for the absorption of visible light of the solar spectrum for photocatalysis [68]. However, recent studies on MXenes and MXene-based materials show high electrical conductivity, large specific surfaces, and abundant metal exposure. MXenes and MXene-based have the potential as a cocatalyst to develop photocatalytic activity by enhancing the partitioning of photoexcited charge carriers [152]. MXenes are not usually semiconductors and due to their high electrical conductivity, they can provide an excellent platform for semiconducting materials to create composite/heterostructure photocatalysts. So, during photocatalysis, irradiation excites electrons in the semiconductor and photogenerated electrons flow into the conduction band quickly because MXene has a promising electron-trapping property that lets electrons and holes partition efficiently. The electrons from the MXenes layers interact with oxygen to produce O_2^-, while the h^+ interacts with water to produce OH radicals [153]. Carbon dioxide and water are both formed when superoxide radicals and hydroxyl radicals react with pollutant molecules [154]. The present review analyzes the use of MXenes in the field of photocatalysis from four research sections: hydrogen evolution reactions (HER), CO_2 reduction reactions (CO_2RR), N_2 fixation, and pollutant degradation.

4.2. Photocatalytic hydrogen evolution

As global warming and energy shortages affect human life globally, they have become worldwide concerns during the last few decades. H_2 gas is a clean combustion fuel and offers a higher energy density compared to fossil fuels, making it an ideal energy source to replace fossil fuels [155, 156]. The energy density of diesel is 45.5 mega joules per kilogram (MJ kg^{-1}), which is slightly lower than the energy density of gasoline, which is 45.8 MJ kg^{-1}. The energy density of hydrogen is approximately 120 MJ kg^{-1}, almost three times greater than that of diesel or gasoline [157]. Water electrolysis, coal gasification, electrocatalysis, and photocatalysis are four main methods that are used to prepare H_2 to date. Photocatalytic H_2 evolution is considered promising because it is sustainable and does not produce secondary pollutants [155]. H_2 evolution process consists of three steps, namely, (a) the initial formation of $h^+ + e^-$ (b) the production of H^* and (c) the formation of 1/2 H_2. H^* adsorption state directly impacts the final hydrogen evolution efficiency in step (c) and is one of the most important factors that can be represented by

the Gibbs adsorption free energy $|\Delta G_{H^*}|$ [158]. As of today, a large number of photocatalysts, including metal sulfides, titanium dioxide (TiO_2), barium titanate ($BaTiO_3$), g-C_3N4, and $Sr_2Ta_2O_7$, have been investigated for H_2 evolution [159]. However, the photocatalysts exhibit relatively low light utilization capacity and fast recombination of photogenerated carriers, which limits their practical application [160]. In this context, the development of new photocatalysts for H_2 evolution has great significance.

In recent years, MXenes have been reongnized as promising candidates for photocatalytic H_2 production [69, 140]. Based on simulation calculations, it was discovered that $\Delta G_{H^*} = 0.927$ eV when all $Ti_3C_2T_x$ surface groups are –F, and strong adsorption occurs. A catalyst with all surface groups as –O has a $|\Delta G_{H^*}|$ of 0.003 eV, which is superior to the commonly used catalyst Pt (ΔG_{H^*}–0.090 eV). The most desirable value for $|\Delta G_{H^*}|$ should be zero [161, 162]. Apart from contributing to the three steps of HER, $Ti_3C_2T_x$ can also assist in electron–hole separation because of the hydrophilic group on its surface, suitable Gibbs adsorption free energies, and excellent electron transfer efficiency [69, 163]. MXenes anchored onto the monolayer of $Ti_3C_2T_x$ were used as photocatalysts that enabled the photocatalytic evolution of H_2 over TiO_2. The effects of $Ti_3C_2T_x$ on the photocatalytic activity of TiO_2 were evaluated, by irradiating various $TiO_2/Ti_3C_2T_x$ nanocomposites with light and using CH_3OH as a hole scavenger for photocatalytic H_2 evaluation [164]. In general, $TiO_2/Ti_3C_2T_x$ nanocomposites displayed better photocatalytic performance than pure TiO_2, because of $Ti_3C_2T_x$'s ability to separate photoinduced charge carriers. In the presence of 5% monolayer $Ti_3C_2T_x$, the maximum amount of H_2 was produced (2.71 mmol g^{-1} h^{-1}) that was approximately nine times greater than that of pure TiO_2 particles (0.29 mmol g^{-1} h^{-1}). This is due to the enhanced separation of photogenerated e^-/h^+ in TiO_2, as verified by photoluminescence and transient photocurrent responses, as well as electrochemical impedance spectrum measurements [165]. Additionally, quantum dot (QDs) $Ti_3C_2T_x$ or monolayer $Ti_3C_2T_x$ are both more active in H_2 evolution.

As a hole scavenger, lactic acid was used to study the effect of MXene on the photocatalytic hydrogen production of ZnCdS under visible light irradiation. Compared with ZnCdS nanoparticles and TM, ZTNM composites improved the efficiency of photocatalytic hydrogen production significantly, and the optimal hydrogen production efficiency of ZTNM-3 was 3.3 times that of ZnCdS nanoparticles [166].

Despite its advantages, monolayer $Ti_3C_2T_x$ has several disadvantages such as (a) its preparation is complex, (b) the catalyst has low structural stability and is easily oxidized, and (c) monolayer or few-layer structures are difficult to manipulate. At present, few-layered structures are fabricated electrostatically (self-assembly) or using *in situ* growth. *In situ* growth significantly improves the stability of composite catalysts over electrostatic self-assembly [69, 155, 167]. Xiao *et al* [168] fabricated a 1D/2D CdS/Ti_3C_2 heterojunction by *in situ* solvothermal methods for H_2 generation. 1D/2D Schottky heterojunctions between CdS and Ti_3C_2 provide accelerated charge separation as well as a lower Schottky barrier for solar-driven hydrogen evolution from water splitting due to their specific interface characteristics. The CdS/Ti_3C_2 nanosheets are seven times more active than the CdS nanorods in photocatalytic hydrogen evolution suggesting a synergistic response between n-type semiconductor CdS and 2D Ti_3C_2 MXene. Yang *et al* [169] found that Ti_3C_2 MXene@TiO_2/$CuInS_2$ (M@T/CIS) exhibited a 356.27 μmol g^{-1} h^{-1} rate of H_2 evolution, which is 69 and 636 times higher than that of M@T and CIS, respectively, highlighting its potential as photocatalysts for H_2 evolution. The following synergistic effects were attributed to the enhanced photocatalytic H_2 evolution activity increased light-harvesting ability, enhanced charge separation by Ti_3C_2/CIS Schottky junction and large number of active sites on the surface of Ti_3C_2 MXene, due to its numerous functional groups.

In a recent study, photocatalytic H_2 evolution over hierarchical $Ti_3C_2T_x$ MXene@In_2S_3-NiS is presented in which NiS is coupled with a Schottky heterojunction of $Ti_3C_2T_x$ MXene@In_2S_3 using photodepotition technique as sown in the figure 6 [170]. Morphology of the synthesized nanocomposites are is depicted in the SEM and TEM images as shown in the figures 6(a)–(c). It was reported that H_2 generation rate over the optimized In_2S_3-3%NiS was approximately 29.0 times higher that that of bare In_2S_3 (figure 6(e)). Coupling of MXebe to form $Ti_3C_2T_x$ MXene@In_2S_3-NiS nanocomposites resulted in further improvement in H_2 generation (figure 6(f)). In another study, Huang *et al* [171] prepared P-doped tubular g-C_3N_4/Ti_3C_2 (PTCN/TC) MXene by self-assembly approach. The H_2 evolution rate was highest for PTCN/TC (2.20 μmol g^{-1} h^{-1}), as it was 4.3 and 2.0 times higher than that of pure bulk g-C3N4 and PTCN, respectively. The metallic Ti_3C_2 served as a sink for electrons and a collector for photons in this composite. Furthermore, ultrathin Ti_3C_2 flakes that showed exposed terminal metal sites as a co-catalyst displayed higher photocatalytic reactivity in H_2 evolution than carbon materials. Very recently, Cao *et al* [172] reported the successful fabrication of MXene/ZnxCd1-xS photocatalysts for H_2 evolution. The resulting photocatalysts provided excellent photocatalytic performance, with the best rate of H_2 evolution at 14.17 mmol g^{-1} h^{-1}. High-efficiency photocatalysis is attributed to the enhanced separation ability of photocarriers and optimal band structure with enhanced oxidation capacity of the valence band of MXene/ZnxCd1-xS photocatalysts. As shown in table 3, $Ti_3C_2T_x$ results in a greater

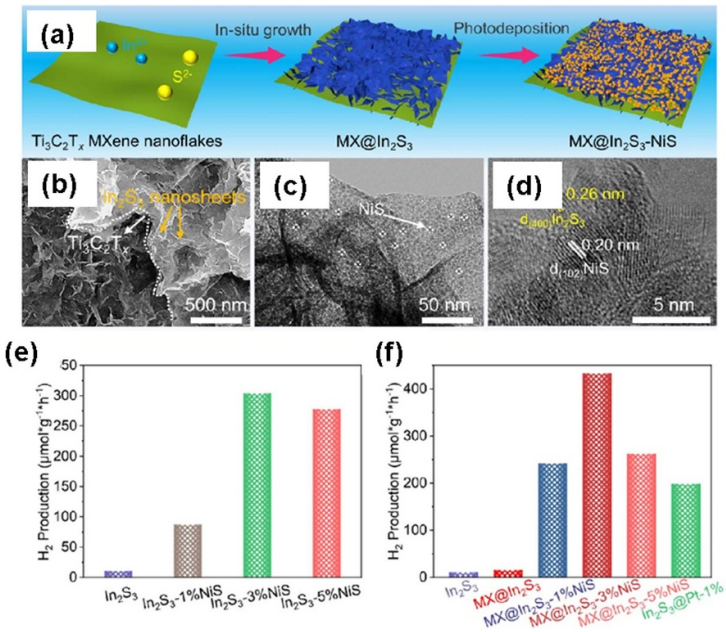

Figure 6. (a) Fabrication of MX@In_2S_3-NiS ternary heterostructures. (a) Schematic illustration for the fabrication of MX@In_2S_3-NiS ternary heterostructures. (b) FESEM. (a), (b) Reproduced from [170]. © IOP Publishing Ltd All rights reserved. (c) and (d) TEM images of the composite. (e) Comparison of H_2 generation rates over bare In_2S_3 and In_2S_3-NiS composites. (f) Over bare In_2S_3, MX@ In_2S_3-NiS, and In_2S_3-Pt composites.

Table 3. Photocatalytic hydrogen production of various MXenes- based photocatalysts.

Photocatalysis	Sacrificial agent	Light source	H_2 production rate (mmol g^{-1} h^{-1})	Improvement times (bare catalysts)	References
$Cd_{0.5}Zn_{0.5}S/Ti_3C_2$	Na_2SO_3/Na_2S	300 W Xenon lamp	9.07	33 (traditional Pt)	[174]
Ti_3C_2 MXene@$TiO_2/ZnIn_2S_4$	Na_2S/Na_2SO_3	300 W Xenon lamp	1.18	9.1 and 4.6 (M@TiO_2 and pure ZIS, respectively)	[175]
PtO@Ti_3C_2/TiO_2	—	300 W Xenon lamp	2.54	3 (TiO_2)	[176]
1D CdS/2D Nb_2CT_x	Methanol	Visible light	5.30	1.7 (CdS)	[177]
$Zn_mIn_2S_{m+3}$ ($m = 1$–3)/MXene	Triethanolamine (TEOA)	300 W Xenon lamp	3.04	2.67 ($Zn_2In_2S_5$)	[178]
HCN/Ti_3C_2	TEOA	3 W LED	4.22	2 and 8 (HCN and BCN, respectively)	[179]
$Ti_3C_2/SnNb_2O_6$	Methanol	300 W Xenon lamp	0.17	2 (SNO nanoplate)	[180]
$Cd_xZn_{1-x}S/Ti_3C_2$	Na_2S/Na_2SO_3	300 W Xenon lamp	15.03	2.7 (CZS)	[181]
BQ/Ti_3C_2/ultrathin g-C_3N_4 (BQ/TiC/UCN)	TEOA	300 W Xenon lamp	18.42	47.2 and 19.4 (BCN and UCN, respectively)	[182]
Protonated g-$C_3N_4/Ti_3C_2T_x$	—	300 W Xenon lamp	0.98	3.5 (protonated g-C_3N_4)	[183]
C-TiO_2/g-C_3N_4	TEOA	300 W Xenon lamp	1.409	24 and 8 (TiO_2 and g-C_3N_4, respectively)	[184]
Protonated g-C_3N_4/Ti_3C_2	TEOA	300 W Xenon lamp	2.18	2.5 and 2.6 (g-C_3N_4 and g-C_3N_4)	[185]
Ti_3C_2/g-C_3N_4	—	200 W Hg lamp	0.072	10 (g-C_3N_4)	[186]

yield of H_2 compared to the base catalyst alone. In summary, hydrogen production doubled after loading with $Ti_3C_2T_x$. The reason for this incredible promotion is mainly due to the following three aspects of $Ti_3C_2T_x$, (a) it provides a high throughput channel as a co-catalyst during which the excited electrons can pass through while holes cannot, (b) its hydrophilicity, and (c) its adsorption on hydrogen has a Gibbs free energy of zero. It is important to dedicate more resources to studying MXene QDs as opposed to their

sheet counterparts. Thus, a greater understanding of MXene QDs and their influence on activity is highly desired both from an experimental and computation perspective.

4.3. Photocatalytic reduction of CO_2

Photocatalytic CO_2 reduction has received enormous attention in recent decades to simultaneously address the greenhouse effect and the energy shortage. The conversion of CO_2 into CH_4, CO, CH_3OH, HCHO, and HCOOH has been studied extensively using a variety of photocatalysts [187–191]. The reduction of CO_2 with photocatalysts is still challenging due to the low utilization rate of carriers, the low thermodynamic stability of CO_2 molecules, and the insufficient adsorption and activation of CO_2 molecules. Therefore, a highly efficient photocatalyst with high CO_2 reduction activity must be developed [60]. Several recent studies suggested that MXenes may serve as a co-catalyst in photocatalytic CO_2 reduction due to its remarkable physicochemical properties. The potential of MXene for photocatalysis has been demonstrated by numerous theoretical and experimental studies recently [72, 192–194]. The $Ti_3C_2T_x$ MXene-based semiconductor is gaining wide attention as a photocatalytic substrate that is capable of outperforming graphene and noble metals as a co-catalyst in CO_2 reduction.

In addition, $Ti_3C_2T_x$ can allow fast separation of photogenerated charge carriers for light-harvesting materials, which can achieve high photoconversion efficiencies. MXenes offer a large surface area, enriched active adsorption sites, and a good interface contact to allow efficient charge carrier separation [60]. Furthermore, the $Ti_3C_2T_x$ layer exhibits a variety of terminated functional groups, such as O, OH, C, and F, encouraging the need for specific functionalization [72]. Photocatalytic CO_2 reduction follows a five-step process: light adsorption, charge separation, CO_2 adsorption, surface redox reaction, and product desorption [195]. Charge separation occurs during the recombination of electrons and holes when the photocatalyst's CB is greater than the redox potential of CO_2 [69]. There are several factors dictating which of these two competing processes is predominant. As a result of CO_2 adsorption and photogenerated electrons and holes moving from the crystal structure to the surface, the catalyst undergoes a redox reaction. Following the de-attachment of the product, the CO_2 reduction reaction from photocatalysis is completed [196, 197]. Recently, Li *et al* [173] fabricated g-C_3N_4/MXene (MCT) for photocatalytic CO_2 reduction, which showed excellent performance. As a gray powder, MCT was obtained under an N_2 atmosphere by heating g-C_3N_4 and $Ti_3C_2T_x$ mixed in a 10:3 mass ratio respectively at 250°C for 2 h. After treatment with HF, it is evident that the Al layers in Ti_3AlC_2 have been stripped away. The mesoporous surface morphology of mesoporous g-C_3N_4 allows gas molecules to be adsorbed at numerous sites due to its large surface area. $Ti_3C_2T_x$ has enhanced contact with mesoporous g-C_3N_4 due to their morphologies, that resulted in remarkable improvements in the electron separation as well as the efficiency of multiple electron reactions including CO_2 reduction. As a result of illumination to excite electrons of the semiconductor into the excitation state, $Ti_3C_2T_x$ MXene comprises a capacitor that coordinates heterojunction effects. Due to the rapid transfer of electrons, electrons and holes are separated more easily. The steady rise and stable decline of the photocurrent corresponding to the ON and OFF states of the light, respectively, reflect the improved separation of photogenerated electron–hole pairs in Ti_3C_2 and its electron reservoir capabilities. In this case, Ti_3C_2 MXene is a cocatalyst that enhances charge separation and provides the active sites necessary for the reduction reaction. As a result of the photocatalytic activity of the MCT sample for CO_2 reduction, several organic products were generated, among which CO and CH_4 were the dominant product. Mesoporous MCT produces 2.4 times more CH_4 than mesoporous g-C_3N_4 (MC). This evidences the excellent selectivity and activity of MCT. Additionally, a high-speed electronic system in the MXene catalyst enables MCT to also effectively separate charge carriers [173]. In another study ZnO loaded Ti_3C_2 MXene compsites (Ti_3C_2–OH/ZnO) was synthesized by a facile electrostatic self-assembly method and used as a co-cocatalyst for CO_2 photoreduction [198]. Formation of Ti_3C_2–OH/ZnO composite structure due to electrostatic self-assembly between negatively charged Ti_3C_2–OH and positively charged ZnO was revealed by the SEM and high resulation TEM images (figures 7(a) and (b)). The surface-alkalinized Ti_3C_2–OH/ZnO played an important role in increasing the transfer efficiency of of photoinduced charge carriers and ultimately impoving the CO_2 molecules adsorption, resulting in higher photocatalytic CO_2 reduction as depicted in figure 7(C). It was reported that evolution rates of CO and CH_4 was 30.30 μmol g^{-1} h and 20.33 μmol g^{-1} h, respectively, which are much higher than the earlier reported values.

In another study, Tahir *et al* [199] fabricated 2D porous g-C_3N_4 (PCN) coupled exfoliated 3D $Ti_3C_2T_A$ MXene (TiC) nanosheets with TiO_2 nanoparticle (NPs) via *in-situ* growth in a single step through HF treatment approach (figure 8(a)). Figures 8(b) and (c) depict efficacious fabrication of PCN/TiC which can augment the area of interfacial interaction for facilitating the migration of charge carriers. Importantly, the TiO_2 NPs were visible on the Ti_3C_2 nanosheets. PCN/TiC showed excellent performance for photocatalytic CO_2 reduction by

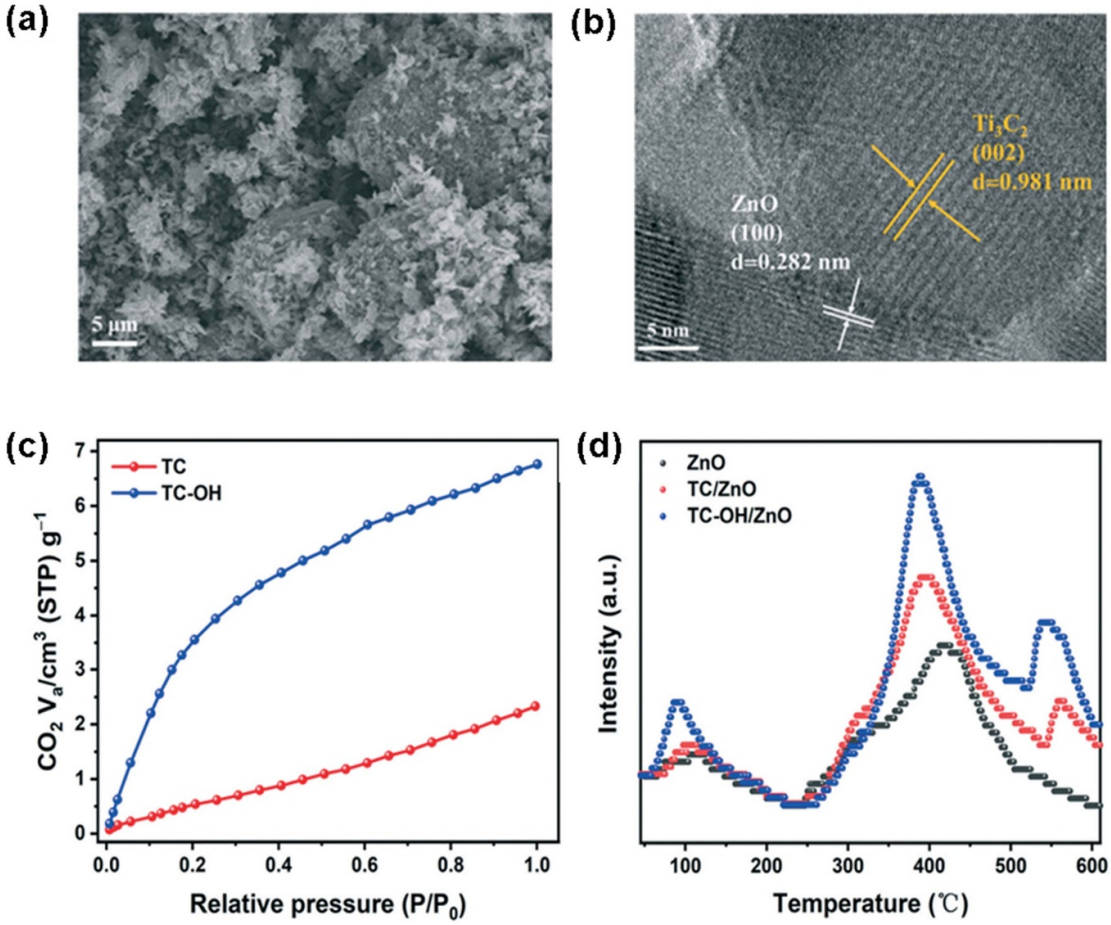

Figure 7. (a) SEM and (b) HR-TEM images of Ti_3C_2–OH/ZnO. (c) CO_2 adsorption behaviors of Ti_3C_2 and Ti_3C_2–OH; (d) CO_2-temperature-programmed desorption spectra of ZnO, Ti_3C_2/ZnO and Ti_3C_2–OH/ZnO. Reprinted from [173], © 2021 Elsevier B.V. All rights reserved.

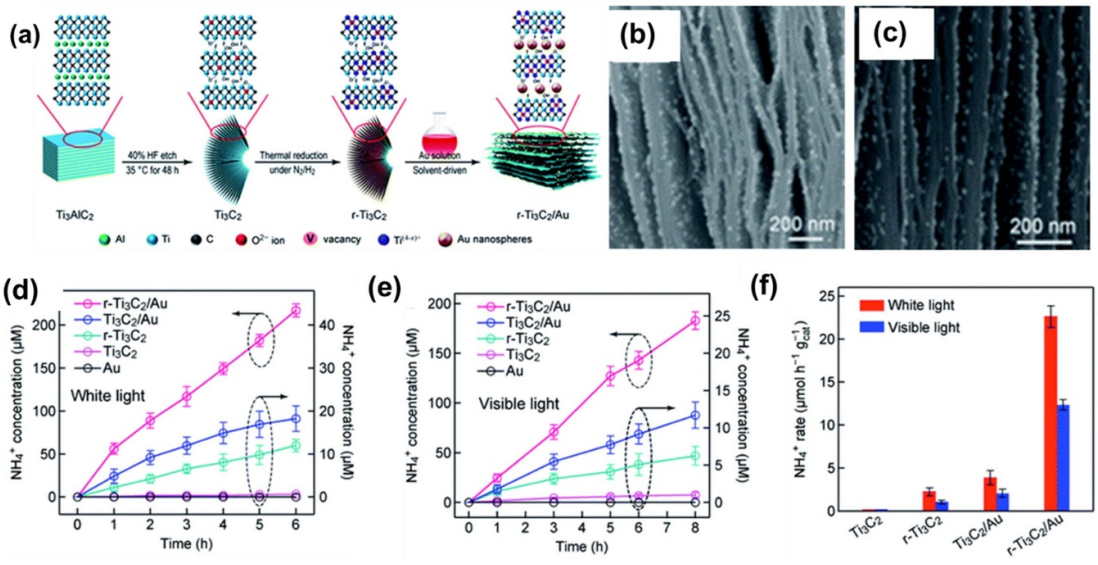

Figure 8. (a) Schematic illustrating the synthesis process. (b) SEM image of Ti_3C_2/Au. (c) SEM image of r-Ti_3C_2/Au. (d) Reaction rate of ammonia concentrations under white light illumination. (e) Reaction of ammonia under visible light exposure. (a)–(e) Reproduced from [210] with permission from the Royal Society of Chemistry. (f) Ammonia production under both lights conditions.

Table 4. Summary of the typical photocatalysts for CO_2 reduction.

Photocatalysts	Light source	Products and yield μmol h^{-1} g^{-1}	Reaction conditions	Activity improvement factor	References
$Cd_{0.2}Zn_{0.8}S@Ti_3C_2$	300 W xenon lamp	CO (3.31) CH_4 (3.51)	30 mg catalyst liquid-solid	—	[201]
TiO_2 A/Ti_3C_2TR	35 W, High intensity discharge (HID) lamp, 8000 K	CO (85) CH_4 (18)		9.53 (CH_4)	[202]
Co–$Ti_3C_2T_x$	300 W xenon lamp	CO (600)	15 mg gas-solid	15	[203]
$TiO_2/C_3N_4/Ti_3C_2$	350 W Xe lamp	(CO) (4.39) CH_4 (1.20)	30 mg catalyst liquid-solid	1.4 (CO)-	[204]
Ti_3C_2/g-C_3N_4	300 W xenon lamp	CO (5.2) CH_4 (0.05)	20 mg catalyst gas-solid	8.4 (CO) 3.0 (CH_4)	[205]
$Ti_3C_2(OH)_2$/g-C_3N_4	300 W xenon lamp	CO (2.3) CH_4 (0.04)	10 mg catalyst gas–liquid	3	[206]
Co–Co LDH/$Ti_3C_2T_x$	5 W LED lamp	CO (6.248)	—	—	[207]
Cu_2O/Ti_3C_2MXene	300 W xenon lamp	CO (17.5)–CH_4 (0.96)	—	3.1 CO 4.0 CH_4	[208]

generating CO and CH_4 products. As compared to TiC-24/PCN, TiC-96/PCN, and PCN composite samples, 10TiC-48/PCN produced CO and CH_4 at the maximum rates of 317.3 and 78.55 μmol g^{-1} h^{-1}. The CO and CH_4 evolution results were 9.9 and 6.7 folds higher using 10 TiC-48/PCN composite than pristine sample PCN (figures 8(d) and (e)). The reason for this is the lower separation efficiency of photogenerated charges with pure PCN, so only a smaller number of electrons can combine effectively with CO_2 for activation of the gas. In composite materials, photoluminescence analysis (PL) is an effective method of investigating charge separation and recombination efficiency. In pristine PCN, PL intensity is very high due to the high recombination probability of the single charge carrier, while the PL emission peaks of samples TiC-24, TiC-48, and TiC-96 are significantly smaller than those of PCN. It might be due to the metallic nature of MXenes as well as its dark color. In contrast, PL intensity was significantly reduced when PCN was anchored to TiC-48 to form a TiC-48/PCN heterojunction composite. The composite samples demonstrate efficient charge carrier separation by using $Ti_3C_2T_x$ MXene decorated with TiO_2 NPs and attached to 2D porous g-C_3N_4 sheets [199]. Moreover, a highly efficient 'storage capacitor' is created when $Ti_3C_2T_x$ forms a heterojunction with g-C_3N_4. Electrons transfer quickly to $Ti_3C_2T_x$ on the semiconductor surface, but holes cannot. As a result, the material's photocatalytic performance is greatly improved, and the electron–hole recombination is greatly reduced. Meanwhile, abundant defects on the surface of $Ti_3C_2T_x$ act as excellent adsorption sites for CO_2 [193]. Low *et al* [200] prepared TiO_2/Ti_3C_2 composite for photocatalytic reduction of CO_2. The TiO_2 was tightly bonded to the Ti_3C_2, and the composites had a rice crust appearance. It was found that the optimized TiO_2/Ti_3C_2 composite produced CH_4 at a higher rate than commercial TiO_2 and also had very good photostability. According to the experimental and theoretical results, Ti_3C_2's ultrahigh electrical conductivity and light absorption properties allowed carriers to be separated efficiently [200].

The above examples show Ti-MXene's potential for highly selective photocatalytic CO_2 conversion, which is a positive signal that they will have broad applications both theoretically and computationally shortly. Thus, coupling various semiconductive photocatalysts to $Ti_3C_2T_x$ requires extensive research. In addition, simulation of a structure with such properties will provide a better understanding of $Ti_3C_2T_x$'s adsorption, activation, and charge transfer mechanisms. However, the use of $Ti_3C_2T_x$ is relatively smaller in photocatalytic reduction of CO_2 than in photocatalytic hydrogen evolution. The reason is because of its instability and the fact that it has its carbon resources, which can interfere with the photocatalytic reduction of CO_2. The results listed in table 4 demonstrate that among limited reports, $Ti_3C_2T_x$ with both single-layered and multilayered structures displays an obvious production enhancement.

4.4. Photocatalytic N_2 fixation

Nitrogen is an essential component of all living organisms in the form of proteins and nucleic acids. Despite the high concentration of nitrogen in the atmosphere, most living organisms are mostly able to use the nitrogen element as ammonia (NH_3) or NO^-_3. In the industrial sector, ammonia is a crucial ingredient in fertilizers and is produced through the Haber-Bosch process, which uses N_2 and H_2 as feedstocks. In

Table 5. Comparison of photocatalysts including MXene for N_2 fixation.

Photocatalysts	Light source	NH_3 production rate (μmol g^{-1} h^{-1})	References
$Bi_4O_5Br_2/Ti_3C_2$	300 W xenon lamp	277.74	[212]
$Nb_2O_5/C/Nb_2C/g\text{-}C_3N_4$	300 W xenon lamp	927.00	[213]
$MXene@TiO_2$	300 W xenon lamp	110.00	[214]
$CdS@Ti_3C_2$	300 W xenon lamp	293.06	[215]
$Ti_3C_2T_x/TiO_2$	300 W xenon lamp	422.00	[216]
$TiO_2@C/g@C_3N_4$	300 W xenon lamp	250.60	[217]

light of the solid bonding between the NN bonds (945 kJ mol^{-1}), such a process requires a high quantity of energy, causing a variety of environmental and energy issues. Recent developments in photocatalytic N_2 fixation utilizing solar energy have been considered a promising option for generating ammonia under mild environmental conditions. In contrast, rapid photogenerated charge carriers and N_2 activation are strongly contested to this technology. Recently, MXene photocatalysts have been used in the photocatalytic N_2 fixation reaction to address these issues.

Recently, Fang *et al* [209] prepared BiOBr/MXene-Ti_3C_2 composite catalysts using electrostatic adsorption and self-assembly. $BiOBr/Ti_3C_2$ prepared in 10 wt.% exhibits the best performance for the photocatalytic fixation of N_2. $BiOBr/Ti_3C_2$ showed up to 234.6 μmol g^{-1} h^{-1} evolution rate of NH_3, which is approximately 48.8 and 52.4 times greater than that of pure BiOBr and Ti_3C_2, respectively. With the presence of designed double oxygen and titanium vacancies for $BiOBr/Ti_3C_2$, localized electrons are capable of adsorbing and activating N_2, having the ability to be reduced to NH_3 by the interfacial electrons of $BiOBr/Ti_3C_2$. Furthermore, the *in-situ* Fourier transform infrared results indicate that continuous protonation processes lead to the generation of N_xH_y species. Additionally, according to density functional theory calculations, titanium vacancies (VTi) induce high absorption energy for nitrogen atoms on the surface of $BiOBr/Ti_3C_2$. Particularly, the P-electron feedback caused by VTi can elongate the N_2 bond by 31.6% by effectively weakening the N≡N triple bond. Moreover, from the above study, the built-in electric field is demonstrated to drive charge transfer at the local interface after the coupling of BiOBr and $Ti_3C_2T_x$. As a result of the electron trap (Schottky junction) between BiOBr and $Ti_3C_2T_x$, a special structure is formed. By capturing and accumulating photosensitive electrons, it can assist in promoting multielectron NRR. On top of that, the large specific Brunauer–Emmett–Teller (BET) surface area of MXene [51] in heterojunction materials and their black appearance can provide a high level of 'reaction sites' and improve the light adsorption capacity [209].

In another study, Chang *et al* [210] employed a controlled solvent-driven approach to synthesize partially reduced layered $Ti_3C_2T_x$ MXene and integrate it with Au nanospheres in a sandwich-like structure (figure 8). There are many low-valence titanium sites on r-$Ti_3C_2T_x$, which serve as active sites for capturing and activating N_2 molecules. By taking advantage of the embedded Au nanospheres, the activated N_2 is reduced with plasmonic hot electrons. It is also important to note that the sandwich architecture prevents the $Ti_3C_2T_x$ layers from self-stacking, allowing the active sites to be exposed for utilization. The r-Ti_3C_2/Au has an incredibly high N_2 photo-fixation activity due to the abundance of $Ti^{(4-x)+}$ active sites and localized surface plasmon resonance (LSPR) effect working together. To utilize Ti_3C_2 MXene for N_2 photo-fixation, the Ti_3C_2 MXene's active sites are important for N_2 adsorption and activation [110]. Similarly, an RuO_2-loaded TiO_2–MXene was developed by Hao *et al* [211] for photocatalytic N_2 fixation. Their method uses TiO_2, $Ti_3C_2T_x$, and RuO_2 as light collectors, electron mediators, and N_2 adsorbents, respectively. In the present study, RuO_2 NPs were primarily located on the $Ti_3C_2T_x$ matrix rather than on TiO_2. Therefore, upon irradiation with light, photogenerated electrons transferred first from TiO_2 to $Ti_3C_2T_x$, and then migrated to RuO_2 for reduction of the adsorbed N_2 on the RuO_2. It is possible that such intermediate photogenerated charge carrier transfers during the sample preparation could contribute to extending the lifetime of the various photogenerated charge carriers. Consequently, $RuO_2/TiO_2/Ti_3C_2$ displayed significantly higher photocatalytic N_2 fixation activity than the TiO_2, RuO_2, TiO_2/Ti_3C_2, and TiO_2/RuO_2, respectively [211]. In short, photocatalytic N_2 fixation using Ti_3C_2-based photocatalysts is a viable way to improve NH_3 production through photocatalytic N_2 fixation. However, MXene-based photocatalysts have been controversial regarding their photocatalytic N_2 fixation mechanism. The key question is how N_2 molecules adsorb on $Ti_3C_2T_x$ MXene. In this regard, future experiments, and studies on the N_2 adsorption model for Ti_3C_2-based photocatalysts are highly desired. Additionally, in general, very little work has been done on MXenes for photocatalytic N_2 fixation, and the yield rate needs to be increased (table 5).

4.5. Photocatalytic degradation of pollutants

Photocatalytic degradation occurs through the generation of oxidizing holes by photocatalytic

semiconductor materials. Oxidation of dissolved oxygen can lead to the formation of superoxide radicals, singlet oxygen, and hydroxyl radicals. It is possible for these species to directly oxidize substrates. The $Ti_3C_2T_x$ material has a wealth of surface groups and active sites, making it a good adsorbent for many substrates. Therefore, $Ti_3C_2T_x$ has been particularly attractive as a photoactive degradation catalyst and has been investigated by several researchers. For example, the photocatalytic structure of ZnCdS/TiO_2/Na-MXene composites was prepared by Qin *et al* [218] to obtain excellent photocatalysts with high photo-corrosion resistance. MXene was wrapped by Na^+ and ZnCdS nanoparticles under hydrothermal conditions, slowing down further oxidation of Ti_3C_2 MXene into TiO_2 and improving MXene utilization. A ZnCdS/TiO_2/Na-MXene composite with an optimal adsorption capacity to methylene blue reached 299.68 mg g^{-1}, confirming that the MXene content was crucial for the removal of an organic dye. The reported adsorption capacity was achieved by performing a dye adsorption experiment under dark conditions. Further, the degradation capabilities of ZnCdS/TiO_2/Na-MXene composite for methylene blue were assessed under UV light and the synthesized composites exhibited excellent photocatalytic degradation of dye in a short period. ZnCdS layer intercalation increased the basal distances in ZnCdS/TiO_2/Na-MXene from 10.59 Å to 15.21 Å, which could encourage the transportation and adsorption of organic pollutants. ZnCdS/TiO_2/Na-MXene showed 9.3 times higher degradation efficiency than pure ZnCdS in 120 min [218]. Another research group preprared $Ti_3C_2T_x$ (001-T/MX) photocatalyst by hydrothermal treatment of $Ti_3C_2T_x$ (MXene) and utilsied it for the photodegradation of carbamazepine (figure 9). The adsorption of of carbamazepine onto pristine MXene and 001-T/MX composite wa about 5% and 7%, respectively, which is very lower removal efficiency (figure 4(c)). Whereas, photodegredation removal rate was very higher under UV light irradiation as showed in the figure 9(b).

Besides, Zou *et al* [219] prepared MXene-Ti_3C_2/MoS_2 composites to be used under visible light illumination for the first time in photocatalytic degradation of ranitidine (RAN) and to reduce nitrosamine dimethylamine (NDMA) formation potential (NDMA-FP). These composites were analyzed in terms of the morphology, chemical composition, and structural properties which revealed the generation of a heterojunction between MoS_2 and $Ti_3C_2T_x$. This separated electron–hole pairs and facilitated charge transfer, resulting in improved photocatalytic performance. MXene-Ti_3C_2/MoS_2 composite showed the highest RAN degradation and mineralization efficiency in 60 min, with an NDMA-FP of 2.01%. The degradation of RAN was greatly aided by radicals, including the radicals $\bullet O_2^-$, h^+, and •OH, but it was the •OH radicals that were responsible for the majority of the photocatalytic activity.

In addition, Sharma *et al* [5] reported 2D ternary ZnO–B_i2WO_6–Ti_3C_2 for photocatalyst degradation of colorless pharmaceutical pollutants. X-ray diffraction confirmed the formation of the individual materials and nanocomposites, while electron microscopy determined the 2D morphology. ZnO–Bi_2WO_6–Ti_3C_2 under sunlight irradiation, exhibited a maximum 77% degradation of ciprofloxacin in 160 min. According to the mechanistic analysis, electrons flow from ZnO and Bi_2WO_6 to $Ti_3C_2T_x$ during nanocomposite formation, indicating that the MXene plays a vital role in separating photogenerated charges and improving the photocatalytic activity. In addition to increasing the efficiency of photogenerated charge carrier separation, Fang *et al* [220] found that $Ti_3C_2T_x$ could enhance the adsorption capacity of Ag_2WO_4 for antibiotic pollutants such as tetracycline hydrochloride and sulfadimidine. The adsorption and photocatalytic reactions were simulated using dark and light conditions, respectively, for testing the removal of antibiotic pollutants. $Ti_3C_2T_x$ showed negligible direct adsorption capacity for pollutants under dark conditions, but it improved the dispersion and prevented the aggregation of Ag_2WO_4, thus increasing its adsorption capacity for antibiotics. Combining enhanced adsorption capacity and improved photogenerated carrier separation efficiency, Ag_2WO_4/$Ti_3C_2T_x$ exhibited significantly higher photocatalytic degradation activity compared to both pristine $Ti_3C_2T_x$ and Ag_2WO_4. Table 6 reports a summary of the photocatalytic degradation of contaminants using MXenes.

5. Recyclability of MXene

The recyclability of MXenes and the ability to retain their properties are among the most important research subjects in terms of efficiency and cost minimization in recent years [221, 222]. The feasibility of regeneration has been demonstrated using hydrochloric acid, HNO_3, or $Ca(NO_3)_2$, alcohol, and thiourea [222–225]. For instance, Khan and Andreescu [222] found that recycling $Ti_3C_2T_x$ with 0.2 M HCl to remove Cs ions resulted in a sorbent removal rate of more than 90%. According to Shahzad *et al*'s [226] experiment, the authors achieved nearly 100% reusability of MX-$SA_{4:20}$ with 8 M hydrochloric acid. In another study, it was found that the MXene/alginate structure is more stable than calcium nitrate crosslinking, which leads to higher absorption rates than non-cross-linked compounds [227]. It is crucial to determine whether a photocatalyst can be stable since its photo-corrosion strictly limits its application [228].

A cycling test was performed for the degradation of antibiotics using the Ag_2WO_4/Ti_3C_2 MXene to verify their reusability. After three cycles, a clear

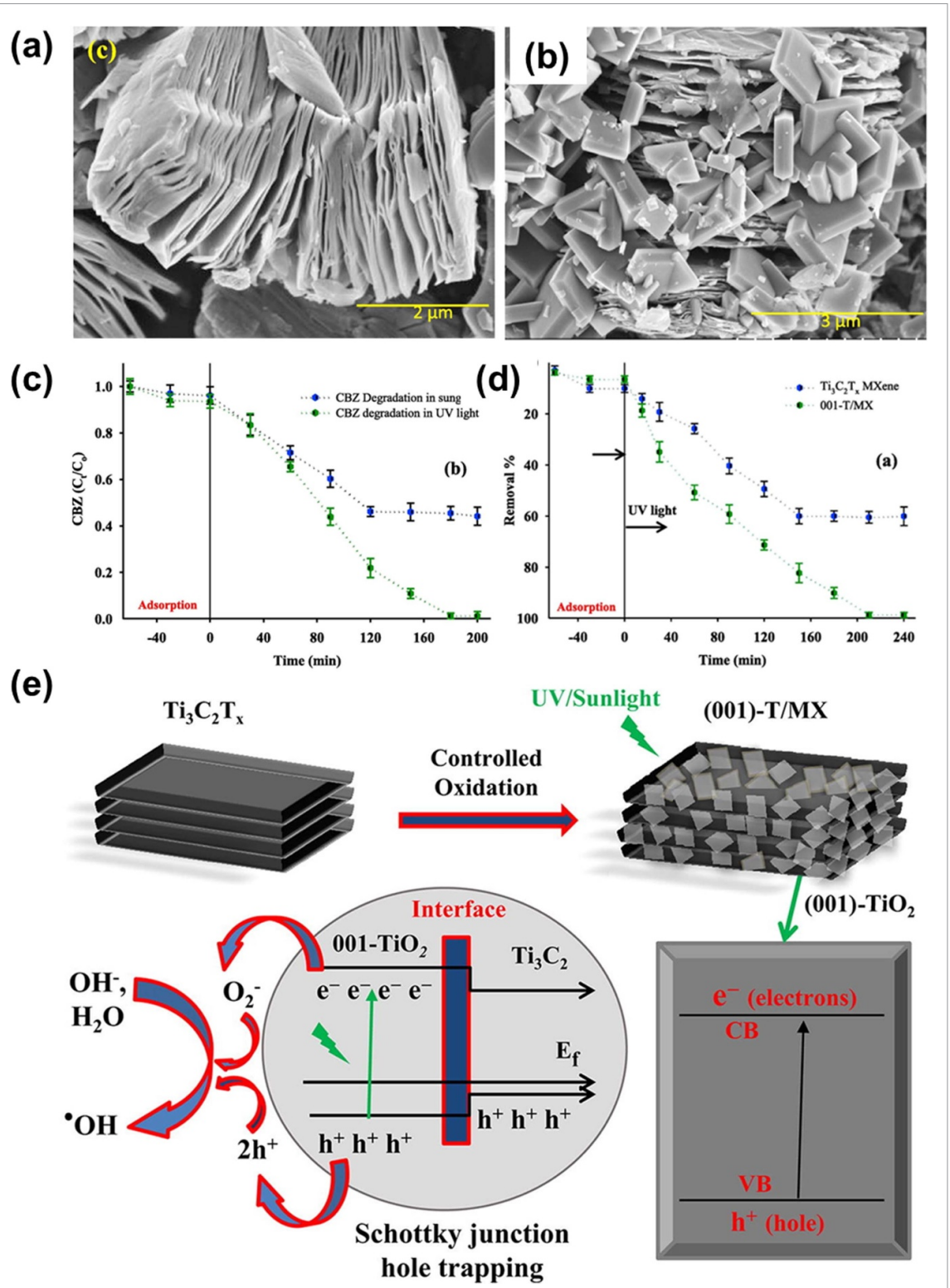

Figure 9. SEM images of (a) $Ti_3C_2T_x$ MXene and (b) 001-T/MX composite photocatalyst. (c) Photodegradation of CBZ by $Ti_3C_2T_x$ MXene and 001-T/MX. (a)–(c) Reprinted from [52], © 2018 Elsevier B.V. All rights reserved. (d) Photocatalytic degradation of CBZ dye under sunlight and UV light irradiation using 001-T/MX photocatalyst.

reduction trend in cyclical production has been observed, as estimated removal efficiencies for tetracycline hydrochloride and sulfadimidine have both declined by approximately 9% and 22%, respectively. Reduction probably occurs as a result of photocorrosion, photolysis, or photocatalyst damage during reuse. It was generally expected that a small amount of Ag would be generated during the initial fabrication of Ag_2WO_4/Ti_3C_2 MXene since the terminal metal sites of Ti_3C_2 MXene exhibit strong oxidation and reduction reactivity. Nevertheless, the XRD patterns of Ag_2WO_4/Ti_3C_2 did not change before and after the reaction, indicating that the MXene maintains good stability [220]. Testing of monolayer

Table 6. Summary of photocatalytic degradation of pollutants.

Photocatalyst	Pollutant	Light Source	Degradation/ removal	References
MXene-Handmade (MX-H)	Methylene Blue	Visible light	98%	[231]
$TiO_2(TiO_{2-x})/Ti_3C_2$ (A-TOTC)	Bisphenol A	Xenon lamp 300 W	90%	[232]
Ti_3C_2	Methylene Blue, rhodamine B and methyl orange	Xenon lamp 300 W	90%, 83.41% and 44.26%	[233]
MXene/NH_2-MIL-88B	Cr(VI) and methyl orange	Visible light	93.4 and 96.9	[234]
MXene/$ZnIn_2S_4$	Rhodamine B	UV light	90	[235]
ZnO/MXene	Rhodamine B	Xenon lamp 300 W	97	[236]
TiO_2@Ti_3C_2	Tetracycline hydrochloride	Visible light	92.1	[237]
Ag/g-C_3N4/Ti_3C_2	Methylene blue and tetracycline hydrochloride,	300 W xenon lamp	>90	[228]
MXene/Ag_2S	Methylene blue	Visible light	94	[238]
$CuFe_2O_4/Ti_3C_2$	Perfluorooctanoic acid	300 W xenon lamp	100	[239]
Ti_3C_2/TiO_2				

$TiO_2/Ti_3C_2T_x$ showed that their photocatalytic H_2 evolution rate dropped from 2.7 to 2.3 mmol g^{-1} h^{-1} after four cycles of reaction [229]. Although $Ti_3C_2T_x$ nanoparticles are generally unstable in water containing dissolved oxygen, $Ti_3C_2T_x$ nanoparticles could be stabilized by removing the dissolved oxygen with Ar gas [230]. Therefore, dissolved O_2 was removed through de-aeration with ultrapure Ar gas before photocatalytic H_2 evolution could occur. $Ti_3C_2T_x$ nanoparticles are less likely to oxidize when exposed to photo-induced e^-. In such reaction circumstances, $Ti_3C_2T_X$ can be fairly constant. An XRD pattern of the used $TiO_2/Ti_3C_2T_x$ after photocatalysis showed no notable change in the crystal structure. Nonetheless, as compared to the clean sample, there was a modest decrease in utilized $TiO_2/Ti_3C_2T_x$ light absorption, likely due to TiO_2 particle detachment from the nanocomposites [165, 229].

6. Challenges and future perspectives

MXenes have been attracting enormous attention in the fields of photocatalysis and many others such as energy storage, ion batteries, and sensor technology. The study of MXenes is still in its early stages, and its prospects are primarily as follows:

(a) To fabricate Ti_3C_2 photocatalysts, a multistep process that combines $Ti_3C_2T_x$ with other composites before hybridizing them is usually utilized, which greatly slows down the fabrication process. There is a need to develop novel fabrication methods to reduce the synthetic time and maximize the feasibility of experiments.
(b) Theoretically, there exists a wide variety of MAX precursors, which can be prepared experimentally, and a larger variety of MXene types must be explored to enrich the MXene family.
(c) Specifically, the problem lies in the instabilities of the composite material, which result in unstable photocatalytic performances. Several existing solutions employ single-layer or few-layer structured materials.
(d) MXenes band structure must be explored to expand the material chemistry, structural diversity, and potential applications of these materials. MXenes are predicted to be direct band gap semiconductors theoretically, but their experimental synthesis continues to present challenges.
(e) Till date, research activities have been focused on hydrogen evolution and pollutant degradation, but little research has been accomplished on oxygen evolution, water splitting total, oxygen reduction, etc.
(f) The development of more active composite catalysts should be prioritized, as well as extending their application to other emerging fields.
(g) MXenes can be paired with efficient and cheap semiconductors to enhance their photocatalytic performance and commercial viability.

Further applications of $Ti_3C_2T_x$ MXene in photocatalysis depend upon the material's development. Various methods to enhance the stability of the $Ti_3C_2T_x$ MXene structure should be investigated, starting with synthetic approaches. Moreover, $Ti_3C_2T_x$ MXene should be further explored for its hydrophilicity as well as its rich surface groups, particularly in liquid phase photocatalysis.

Since the first report of MXenes in 2011, this research area has been growing rapidly. In recent years, MXenes have received considerable attention for photocatalytic applications for their inherent characteristics, which include superior hydrophilicity, metal-like conductivity, large surface area to volume ratio, excellent microwave absorbing properties, and rich surface chemistry. In this review, we have summarized the recent development of synthesizing $Ti_3C_2T_x$ MXenes, and $Ti_3C_2T_x$-based photocatalysts for different environmental decontamination applications such as hydrogen evolution,

reduction of CO_2, N_2 fixation, degradation of pollutants, and water splitting. Even though $Ti_3C_2T_x$ 2D MXene has been studied for many years, there is still much to learn about its photocatalytic behavior and applications. Considering its numerous advantages and characteristics, $Ti_3C_2T_x$ is a compound that needs further investigation, and it is expected to play a very significant role in the field of photocatalysis.

Data availability statement

All data that support the findings of this study are included within the article (and any supplementary files).

Acknowledgments

The authors K R and K A M are thankful to the Qatar Environment and Energy Research Institute at the Hamad Ben Khalifa University of Qatar Foundation for supporting this research. Also A S and T S gratefully acknowledge funding from the ÅForsk Foundation (Grant No. 21-231), Stiftelsen Olle Engkvist Byggmästare (Grant No. 214-0346), and the Swedish Research Council (Grant Nos. 2017-05030 and 2021-03675).

ORCID iDs

Kashif Rasool https://orcid.org/0000-0002-7759-8448
Khaled A Mahmoud https://orcid.org/0000-0003-1246-4067
Tapati Sarkar https://orcid.org/0000-0003-4754-2504
Asif Shahzad https://orcid.org/0000-0002-1578-6670

Reference

[1] Sharma S K *et al* 2021 MXenes based nano-heterojunctions and composites for advanced photocatalytic environmental detoxification and energy conversion: a review *Chemosphere* **291** 132923
[2] Imran M *et al* 2020 UV light enabled photocatalytic activity of α-Fe_2O_3 nanoparticles synthesized via phase transformation *Mater. Lett.* **258** 126748
[3] Wang P, Lu X, Boyjoo Y, Wei X, Zhang Y, Guo D, Sun S and Liu J 2020 Pillar-free TiO_2/Ti_3C_2 composite with expanded interlayer spacing for high-capacity sodium ion batteries *J. Power Sources* **451** 227756
[4] Varnagiris S, Urbonavicius M, Tuckute S and Lelis M 2021 Formation of Zn-rich ZnO films with improved bulk and surface characteristics by approach of magnetron sputtering technique *Thin Solid Films* **738** 138967
[5] Sharma V, Kumar A, Kumar A and Krishnan V 2022 Enhanced photocatalytic activity of two dimensional ternary nanocomposites of ZnO–Bi_2WO_6–Ti_3C_2 MXene under natural sunlight irradiation *Chemosphere* **287** 132119
[6] Zhang R *et al* 2021 Controlled engineering of tunable 3D-BiOX (X= Cl, Br) hierarchical nanostructures via dopamine-mediated synergetic interactions for efficient visible-light absorption photocatalysis *Appl. Surf. Sci.* **574** 151683
[7] Hong L-F *et al* 2020 Recent progress of two-dimensional MXenes in photocatalytic applications: a review *Mater. Today Energy* **18** 100521
[8] Huang Y *et al* 2016 Bifunctional catalytic material: an ultrastable and high-performance surface defect CeO_2 nanosheets for formaldehyde thermal oxidation and photocatalytic oxidation *J. Environ. Manage.* **181** 779–87
[9] Ahn S *et al* 2020 A 2D titanium carbide mxene flexible electrode for high-efficiency light-emitting diodes *Adv. Mater.* **32** 2000919
[10] Seredych M *et al* 2022 Delamination of MXenes using bovine serum albumin *Colloids Surf.* A **641** 128580
[11] You Z, Liao Y, Li X, Fan J and Xiang Q 2021 State of the art recent progress in MXene-based photocatalysts: a comprehensive review *Nanoscale* **13** 9463–504
[12] Biswal L *et al* 2021 Recent progress on strategies for the preparation of 2D/2D MXene/gC_3N_4 nanocomposites for photocatalytic energy and environmental applications *Catal. Sci. Technol.* **11** 1222
[13] Novoselov K S *et al* 2004 Electric field effect in atomically thin carbon films *Science* **306** 666–9
[14] Nakhanivej P *et al* 2019 Revealing molecular-level surface redox sites of controllably oxidized black phosphorus nanosheets *Nat. Mater.* **18** 156–62
[15] Jaramillo-Fierro X, González S, Jaramillo H A and Medina F 2020 Synthesis of the $ZnTiO_3/TiO_2$ nanocomposite supported in ecuadorian clays for the adsorption and photocatalytic removal of methylene blue dye *Nanomaterials* **10** 1891
[16] Jin C *et al* 2019 Observation of moiré excitons in WSe_2/WS_2 heterostructure superlattices *Nature* **567** 76–80
[17] Yang C, Huang H, He H, Yang L, Jiang Q and Li W 2021 Recent advances in MXene-based nanoarchitectures as electrode materials for future energy generation and conversion applications *Coord. Chem. Rev.* **435** 213806
[18] Dixit F *et al* 2022 Application of MXenes for water treatment and energy-efficient desalination: a review *J. Hazard. Mater.* **423** 127050
[19] Bhat A *et al* 2021 Prospects challenges and stability of 2D MXenes for clean energy conversion and storage applications *2D Mater.* **5** 1–21
[20] Tahir M, Sherryna A, Mansoor R, Khan A A, Tasleem S and Tahir B 2022 Titanium carbide MXene nanostructures as catalysts and cocatalysts for photocatalytic fuel production: a review *ACS Appl. Nano Mater.* **5** 18–54
[21] Ghodbane M, Said Z, Tiwari A K, Syam Sundar L, Li C and Boumeddane B 2022 4E (energy, exergy, economic and environmental) investigation of LFR using MXene based silicone oil nanofluids *Sustain. Energy Technol.* **49** 101715
[22] Thirumal V, Yuvakkumar R, Senthil Kumar P, Ravi G and Velauthapillai D 2022 Facile preparation and characterization of MXene@ platinum nanocomposite for energy conversion applications *Fuel* **317** 123493
[23] Yang M, Yang Z, Lv C, Wang Z, Lu Z, Lu G, Jia X and Wang C 2022 Electrospun bifunctional MXene-based electronic skins with high performance electromagnetic shielding and pressure sensing *Compos. Sci. Technol.* **221** 109313
[24] Miao Z, Chen X, Zhou H, Liu P, Fu S, Yang J, Gao Y, Ren Y and Rong D 2022 Interfacing MXene flakes on a magnetic fiber network as a stretchable, flexible, electromagnetic shielding fabric *Nanomaterials* **12** 20
[25] Liang L, Yao C, Yan X, Feng Y, Hao X, Zhou B, Wang Y, Ma J, Liu C and Shen C 2021 High-efficiency electromagnetic interference shielding capability of magnetic $Ti_3C_2T_x$ MXene/CNT composite film *J. Mater. Chem.* A **9** 24560–70
[26] Wang Y, Qi Q, Yin G, Wang W and Yu D 2021 Flexible, ultralight, and mechanically robust waterborne polyurethane/$Ti_3C_2T_x$ MXene/nickel ferrite hybrid aerogels for high-performance electromagnetic interference shielding *ACS Appl. Mater. Interfaces* **13** 21831–43

[27] Rasheed T 2022 MXenes as an emerging class of two-dimensional materials for advanced energy storage devices *J. Mater. Chem.* A **10** 4558–84

[28] Ezika A C, Sadiku E R, Idumah C I, Ray S S and Hamam Y 2022 On energy storage capacity of conductive MXene hybrid nanoarchitectures *J. Energy Storage* **45** 103686

[29] Liu Y-H, Wang C-Y, Yang S-L, Cao F-F and Ye H 2022 3D MXene architectures as sulfur hosts for high-performance lithium-sulfur batteries *J. Energy Chem.* **66** 429–39

[30] Aslam M K *et al* 2021 2D MXene materials for sodium ion batteries: a review on energy storage *J. Energy Storage* **37** 102478

[31] Xu X *et al* 2021 Progress and perspective: mXene and MXene-based nanomaterials for high-performance energy storage devices *Adv. Electron. Mater.* **7** 2000967

[32] Lipton J, Weng G-M, Alhabeb M, Maleski K, Antonio F, Kong J, Gogotsi Y and Taylor A D 2019 Mechanically strong and electrically conductive multilayer MXene nanocomposites *Nanoscale* **11** 20295–300

[33] Mahmood M, Zulfiqar S, Warsi M F, Aadil M, Shakir I, Haider S, Agboola P O and Shahid M 2022 Nanostructured V_2O_5 and its nanohybrid with MXene as an efficient electrode material for electrochemical capacitor applications *Ceram. Int.* **48** 2345–54

[34] Chen J, Chen H, Chen M, Zhou W, Tian Q and Wong C-P 2022 Nacre-inspired surface-engineered MXene/nanocellulose composite film for high-performance supercapacitors and zinc-ion capacitors *J. Chem. Eng.* **428** 131380

[35] Yu L, Xiong Z, Zhang W, Wang D, Shi H, Wang C, Niu X, Wang C, Yao L and Yan X 2022 SnO_2/SnS_2 heterostructure@ MXene framework as high performance anodes for hybrid lithium-ion capacitors *Electrochim. Acta* **409** 139981

[36] Xue J *et al* 2022 Self-assembled $Ti_3C_2T_x$-MXene/PTh composite electrodes for electrochemical capacitors *J. Mater. Sci., Mater. Electron.* **33** 1–10

[37] Vankayala R *et al* 2022 MXenes and their composites for medical and biomedical applications *Mxenes and Their Composites* (Amsterdam: Elsevier) pp 499–524

[38] Huang H *et al* 2022 Biomedical engineering of two-dimensional MXenes *Adv. Drug. Deliv. Rev.* **184** 114178

[39] Iravani S and Varma R S 2021 MXenes and MXene-based materials for tissue engineering and regenerative medicine: recent advances *Adv. Mater.* **2** 2906–17

[40] Lu B, Zhu Z, Ma B, Wang W, Zhu R and Zhang J 2021 2D MXene nanomaterials for versatile biomedical applications: current trends and future prospects *Small* **17** 2100946

[41] Huang J, Li Z, Mao Y and Li Z 2021 Progress and biomedical applications of MXenes *Nano Sel.* **2** 1480–508

[42] Huifeng X *et al* 2021 Novel two-dimensional MXene for biomedical applications *Prog. Chem.* **33** 752

[43] Tang Y, Yang C, Xu X, Kang Y, Henzie J, Que W and Yamauchi Y 2022 MXene nanoarchitectonics: defect-engineered 2D MXenes towards enhanced electrochemical water splitting *Adv. Energy Mater.* **12** 2103867

[44] Sharma K *et al* 2022 Recent progress on MXenes and MOFs hybrids: structure, synthetic strategies and catalytic water splitting *Int. J. Hydrog. Energy* accepted (https://doi.org/10.1016/j.ijhydene.2022.01.004)

[45] Qiao J *et al* 2021 Research progress of MXene-based catalysts for electrochemical water-splitting and metal-air batteries *Energy Storage Mater.* **43** 509–30

[46] Chang H, Li X, Shi L, Zhu Y-R and Yi T-F 2021 Towards high-performance electrocatalysts and photocatalysts: design and construction of MXenes-based nanocomposites for water splitting *Chem. Eng. J.* **421** 129944

[47] Wang J, Wei X, Song W, Shi X, Wang X, Zhong W, Wang M, Ju J and Tang Y 2021 Plasmonic enhancement in water splitting performance for NiFe layered double hydroxide-N10TC MXene heterojunction *ChemSusChem* **14** 1948–54

[48] Kwon O *et al* 2022 A Comprehensive Review of MXene-based Water-treatment Membranes and Technologies: Recent Progress and Perspectives *Desalination* **522** 115448

[49] Ma X-Y, Fan T-T, Wang G, Li Z-H, Lin J-H and Long Y-Z 2022 High performance GO/MXene/PPS composite filtration membrane for dye wastewater treatment under harsh environmental conditions *J. Compos. Commun.* **29** 101017

[50] Wang Y *et al* 2022 $Ti_3C_2T_x$ MXene nanoflakes embedded with copper indium selenide nanoparticles for desalination and water purification through high-efficiency solar-driven membrane evaporation *ACS Appl. Mater. Interfaces* **14** 5876–86

[51] Shahzad A *et al* 2017 Two-dimensional $Ti_3C_2T_x$ MXene nanosheets for efficient copper removal from water *ACS Sustain. Chem. Eng.* **5** 11481–8

[52] Shahzad A, Rasool K, Nawaz M, Miran W, Jang J, Moztahida M, Mahmoud K A and Lee D S 2018 Heterostructural TiO_2/$Ti_3C_2T_x$ (MXene) for photocatalytic degradation of antiepileptic drug carbamazepine *Chem. Eng. J.* **349** 748–55

[53] Saeed M A *et al* 2022 2D MXene: a potential candidate for photovoltaic cells? A critical review *Adv. Sci.* **9** 2104743

[54] Irfan M *et al* 2021 Synthesis and characterization of manganese-modified black TiO_2 nanoparticles and their performance evaluation for the photodegradation of phenolic compounds from wastewater *Materials* **14** 7422

[55] Mathis T S, Maleski K, Goad A, Sarycheva A, Anayee M, Foucher A C, Hantanasirisakul K, Shuck C E, Stach E A and Gogotsi Y 2021 Modified MAX phase synthesis for environmentally stable and highly conductive Ti_3C_2 MXene *ACS Nano* **15** 6420–9

[56] Seredych M *et al* 2019 High-temperature behavior and surface chemistry of carbide MXenes studied by thermal analysis *Chem. Mater.* **31** 3324–32

[57] Hermawan A, Hasegawa T, Asakura Y and Yin S 2021 Enhanced visible-light-induced photocatalytic NO_x degradation over (Ti, C)-BiOBr/$Ti_3C_2T_x$ MXene nanocomposites: role of Ti and C doping *Sep. Purif. Technol.* **270** 118815

[58] Im J K, Sohn E J, Kim S, Jang M, Son A, Zoh K-D and Yoon Y 2021 Review of MXene-based nanocomposites for photocatalysis *Chemosphere* **270** 129478

[59] Kuang P, Low J, Cheng B, Yu J and Fan J 2020 MXene-based photocatalysts *J. Mater. Sci. Technol.* **56** 18–44

[60] Zhong Q, Li Y and Zhang G 2021 Two-dimensional MXene-based and MXene-derived photocatalysts: recent developments and perspectives *Chem. Eng.* **409** 128099

[61] Soni V, Singh P, Phan Quang H H, Parwaz Khan A A, Bajpai A, Van Le Q, Thakur V K, Thakur S, Nguyen V-H and Raizada P 2022 Emerging architecture titanium carbide ($Ti_3C_2T_x$) MXene based photocatalyst toward degradation of hazardous pollutants: recent progress and perspectives *Chemosphere* **293** 133541

[62] Li K, Lu X, Zhang Y, Liu K, Huang Y and Liu H 2020 Bi_3TaO_7/Ti_3C_2 heterojunctions for enhanced photocatalytic removal of water-borne contaminants *Environ. Res.* **185** 109409

[63] Huang K, Li C, Li H, Ren G, Wang L, Wang W and Meng X 2020 Photocatalytic applications of two-dimensional Ti_3C_2 MXenes: a review *ACS Appl. Nano Mater.* **3** 9581–603

[64] Deysher G *et al* 2019 Synthesis of Mo_4VAlC_4 MAX phase and two-dimensional Mo_4VC_4 MXene with five atomic layers of transition metals *ACS Nano* **14** 204–17

[65] Di J, Yan C, Handoko A D, Seh Z W, Li H and Liu Z 2018 Ultrathin two-dimensional materials for photo-and electrocatalytic hydrogen evolution *Mater. Today* **21** 749–70

[66] Lim K R G, Handoko A D, Nemani S K, Wyatt B, Jiang H-Y, Tang J, Anasori B and Seh Z W 2020 Rational design of two-dimensional transition metal carbide/nitride (MXene) hybrids and nanocomposites for catalytic energy storage and conversion *ACS Nano* **14** 10834–64

[67] Prasad C et al 2020 Recent advances in MXenes supported semiconductors based photocatalysts: properties, synthesis and photocatalytic applications J. Ind. Eng. Chem. 85 1–33
[68] Zhang K et al 2021 Insights into different dimensional MXenes for photocatalysis Chem. Eng. J. 424 130340
[69] Li X et al 2021 Applications of MXene ($Ti_3C_2T_x$) in photocatalysis: a review Adv. Mater. 2 1570–94
[70] Naguib M, Kurtoglu M, Presser V, Lu J, Niu J, Heon M, Hultman L, Gogotsi Y and Barsoum M W 2011 Two-dimensional nanocrystals produced by exfoliation of Ti_3AlC_2 Adv. Mater. 23 4248–53
[71] Nguyen T P, Tuan Nguyen D M, Tran D L, Le H K, Vo D-V N, Lam S S, Varma R S, Shokouhimehr M, Nguyen C C and Le Q V 2020 MXenes: applications in electrocatalytic, photocatalytic hydrogen evolution reaction and CO_2 reduction Mol. Catal. 486 110850
[72] Tahir M et al 2021 Titanium carbide (Ti_3C_2) MXene as a promising co-catalyst for photocatalytic CO_2 conversion to energy-efficient fuels: a review Energy Fuels 35 10374–404
[73] Anasori B, Lukatskaya M R and Gogotsi Y 2017 2D metal carbides and nitrides (MXenes) for energy storage Nat. Rev. Mater. 2 1–17
[74] Salim O, Mahmoud K A, Pant K K and Joshi R K 2019 Introduction to MXenes: synthesis and characteristics. J. Mater. Today Chem. 14 100191
[75] Kumar J A et al 2021 Methods of synthesis, characteristics, and environmental applications of Mxene: a comprehensive review Chemosphere 286 131607
[76] Xue Q et al 2017 Photoluminescent Ti_3C_2 MXene quantum dots for multicolor cellular imaging Adv. Mater. 29 1604847
[77] Er D, Li J, Naguib M, Gogotsi Y and Shenoy V B 2014 Ti_3C_2 MXene as a high capacity electrode material for metal (Li, Na, K, Ca) ion batteries ACS Appl. Mater. Interfaces 6 11173–9
[78] Sarycheva A and Gogotsi Y 2020 Raman spectroscopy analysis of the structure and surface chemistry of $Ti_3C_2T_x$ MXene Chem. Mater. 32 3480–8
[79] Wang L, Zhang M, Yang B, Tan J, Ding X and Li W 2021 Recent advances in multidimensional (1D, 2D, and 3D) composite sensors derived from MXene: synthesis, structure, application, and perspective Small Methods 5 2100409
[80] Hope M A, Forse A C, Griffith K J, Lukatskaya M R, Ghidiu M, Gogotsi Y and Grey C P 2016 NMR reveals the surface functionalisation of Ti_3C_2 MXene Phys. Chem. Chem. Phys. 18 5099–102
[81] Yu F, Sorrentino A and Lichtfouse E 2021 Environmental applications of two-dimensional transition metal carbides and nitrides for water purification: a review Environ. Chem. Lett. 19 1–28
[82] Xiao Z, Yang Z, Li Z, Li P and Wang R 2019 Synchronous gains of areal and volumetric capacities in lithium–sulfur batteries promised by flower-like porous $Ti_3C_2T_x$ matrix ACS Nano 13 3404–12
[83] Dixit F, Zimmermann K, Dutta R, Prakash N J, Barbeau B, Mohseni M and Kandasubramanian B 2021 Application of MXenes for water treatment and energy-efficient desalination: a review J. Hazard. Mater. 423 127050
[84] Sokol M, Natu V, Kota S and Barsoum M W 2019 On the chemical diversity of the MAX phases Trends Chem. 1 210–23
[85] Ansori B and Gogotsi Y 2019 2D Metal Carbides and Nitrides (Mxenes): Structure, Properties and Applications (Cham: Springer)
[86] Anasori B and Gogotsi Y 2019 Introduction to 2D transition metal carbides and nitrides (MXenes) 2D Metal Carbides and Nitrides (Mxenes) (Berlin: Springer) pp 3–12
[87] Meng W et al 2021 Advances and challenges in 2D MXenes: from structures to energy storage and conversions Nano Today 40 101273
[88] Naguib M, Barsoum M W and Gogotsi Y 2021 Ten years of progress in the synthesis and development of MXenes Adv. Mater. 33 2103393
[89] Qiu F et al 2021 Synthesis, characterization and microwave absorption of MXene/$NiFe_2O_4$ composites Cream. Int. 47 24713–20
[90] Gao X et al 2021 Synthesis of NiCo-LDH/MXene hybrids with abundant heterojunction surfaces as a lightweight electromagnetic wave absorber Chem. Eng. 419 130019
[91] Shahzad A, Rasool K, Iqbal J, Jang J, Lim Y, Kim B, Oh J-M and Lee D S 2022 MXsorption of mercury: exceptional reductive behavior of titanium carbide/carbonitride MXenes Environ. Res. 205 112532
[92] Lim G P et al 2021 Synthesis, characterization and biophysical evaluation of the 2D Ti_2CT_x MXene using 3D spheroid-type cultures Cream. Int. 47 22567–77
[93] Jolly S, Paranthaman M P and Naguib M 2021 Synthesis of $Ti_3C_2T_z$ MXene from low-cost and environmentally friendly precursors Mater. Today Adv. 10 100139
[94] Zou X et al 2021 A simple approach to synthesis Cr_2CT_x MXene for efficient hydrogen evolution reaction Ceram. Int. 20 100668
[95] Quyen V T, Grummitt L R, Birrell L, Stapinski L, Barrett E L, Boyle J, Teesson M and Newton N C 2021 Advanced synthesis of MXene-derived nanoflower-shaped TiO_2@ Ti_3C_2 heterojunction to enhance photocatalytic degradation of Rhodamine B Environ. Technol. Innov. 21 101286
[96] Guo Y et al 2020 Synthesis of two-dimensional carbide Mo_2CT_x MXene by hydrothermal etching with fluorides and its thermal stability Cream. Int. 46 19550–6
[97] Naguib M, Mashtalir O, Carle J, Presser V, Lu J, Hultman L, Gogotsi Y and Barsoum M W 2012 Two-dimensional transition metal carbides ACS Nano 6 1322–31
[98] Wang J, Shen M, Liu Z and Wang W 2022 MXene materials for advanced thermal management and thermal energy utilization Nano Energy 97 107177
[99] Ibrahim Y, Meslam M, Eid K, Salah B, Abdullah A M, Ozoemena K I, Elzatahry A, Sharaf M A and Sillanpää M 2022 A review of MXenes as emergent materials for dye removal from wastewater Sep. Purif. Technol. 282 120083
[100] Feng X, Yu Z, Sun Y, Long R, Shan M, Li X, Liu Y and Liu J 2021 Review MXenes as a new type of nanomaterial for environmental applications in the photocatalytic degradation of water pollutants Ceram. Int. 47 7321–43
[101] Károlyházy G, Beke D, Zalka D, Lenk S, Krafcsik O, Kamarás K and Gali Á 2020 Novel method for electroless etching of 6H–SiC Nanomaterials 10 538
[102] Zhang C, Ma Y, Zhang X, Abdolhosseinzadeh S, Sheng H, Lan W, Pakdel A, Heier J and Nüesch F 2020 Two-dimensional transition metal carbides and nitrides (MXenes): synthesis, properties, and electrochemical energy storage applications Energy Environ. Mater. 3 29–55
[103] Greaves M et al 2021 Investigating the rheology of 2D titanium carbide (MXene) dispersions for colloidal processing: progress and challenges J. Mater. Res. 36 1–23
[104] Alhabeb M et al 2017 Guidelines for synthesis and processing of two-dimensional titanium carbide ($Ti_3C_2T_x$ MXene) Chem. Mater. 29 7633–44
[105] Mallakpour S, Behranvand V and Hussain C M 2021 MXenes-based materials: structure, synthesis, and various applications Ceram. Int. 47 26585–97
[106] Li J et al 2021 Intercalation-induced reversible electrochromic behavior of two-dimensional $Ti_3C_2T_x$ MXene in organic electrolytes ChemElectroChem 8 151–6
[107] Qin R et al 2021 Two-dimensional transition metal carbides and/or nitrides (MXenes) and their applications in sensors Mater. Today Phys. 21 100527
[108] Rasool K et al 2019 Water treatment and environmental remediation applications of two-dimensional metal carbides (MXenes) Mater. Today 30 80–102
[109] VahidMohammadi A, Rosen J and Gogotsi Y 2021 The world of two-dimensional carbides and nitrides (MXenes) Science 372 6547
[110] Tang R, Xiong S, Gong D, Deng Y, Wang Y, Su L, Ding C, Yang L and Liao C 2020 Ti_3C_2 2D MXene: recent progress

and perspectives in photocatalysis *ACS Appl. Mater. Interfaces* **12** 56663–80
[111] Zhao R, Di H, Wang C, Hui X, Zhao D, Wang R, Zhang L and Yin L 2020 Encapsulating ultrafine Sb nanoparticles in Na+ Pre-intercalated 3D porous $Ti_3C_2T_x$ MXene nanostructures for enhanced potassium storage performance *ACS Nano* **14** 13938–51
[112] Zhang W and Zhang X 2022 The effect of ultrasound on synthesis and energy storage mechanism of $Ti_3c_2T_x$ MXene *Ultrason. Sonochem.* **89** 106122
[113] Li Z, Pepas L, Tasker F, Reidy J and Khalaf Y 2015 Synthesis and thermal stability of two-dimensional carbide MXene Ti_3C_2 *Mater. Sci. Eng.* B **191** 33–40
[114] Halim J *et al* 2016 Synthesis and characterization of 2D molybdenum carbide (MXene) *Adv. Funct. Mater.* **26** 3118–27
[115] Naguib M, Mochalin V N, Barsoum M W and Gogotsi Y 2014 25th anniversary article: mXenes: a new family of two-dimensional materials *Adv. Mater.* **26** 992–1005
[116] Ghidiu M, Lukatskaya M R, Zhao M-Q, Gogotsi Y and Barsoum M W 2014 Conductive two-dimensional titanium carbide 'clay'with high volumetric capacitance *Nature* **516** 78–81
[117] Nan J *et al* 2021 Nanoengineering of 2D MXene-based materials for energy storage applications *Small* **17** 1902085
[118] Wang B *et al* 2021 Booming development and present advances of two dimensional MXenes for photodetectors *Chem. Eng. J.* **403** 126336
[119] Salim O, Canning D and Kabudula C 2019 Introduction to MXenes: synthesis and characteristics *Mater. Today Chem.* **14** 100191
[120] Benchakar M *et al* 2020 One MAX phase, different MXenes: a guideline to understand the crucial role of etching conditions on $Ti_3C_2T_x$ surface chemistry *Appl. Surf. Sci.* **530** 147209
[121] Wu Y *et al* 2021 MXenes: advanced materials in potassium ion batteries *Chem. Eng. J.* **404** 126565
[122] Cheng Y-W *et al* 2018 Two-dimensional, ordered, double transition metal carbides (MXenes): a new family of promising catalysts for the hydrogen evolution reaction *J. Phys. Chem.* C **122** 28113–22
[123] Peng C *et al* 2018 A hydrothermal etching route to synthesis of 2D MXene (Ti_3C_2, Nb_2C): enhanced exfoliation and improved adsorption performance *Ceram. Int.* **44** 18886–93
[124] Chang H *et al* 2021 Towards high-performance electrocatalysts and photocatalyst: design and construction of MXenes-based nanocomposites for water splitting *Chem. Eng. J.* **421** 129944
[125] Shuck C E *et al* 2021 Safe synthesis of MAX and MXene: guidelines to reduce risk during synthesis *ACS Chem. Health Saf.* **28** 326–38
[126] Li T *et al* 2018 Fluorine-free synthesis of high-purity Ti_3C_2Tx (T= OH, O) via alkali treatment *Angew. Chem., Int. Ed. Engl.* **57** 6115–9
[127] Liu H-J and Dong B 2021 Recent advances and prospects of MXene-based materials for electrocatalysis and energy storage *Mater. Today Phys.* **20** 100469
[128] Sun W *et al* 2017 Electrochemical etching of Ti_2AlC to Ti_2CT_x (MXene) in low-concentration hydrochloric acid solution *J. Mater. Chem.* A **5** 21663–8
[129] Wang Z 2021 A review on MXene: synthesis, properties and applications on alkali metal ion batteries *IOP Conf. Ser.: Earth Environ. Sci.* **714** 042030
[130] Li M *et al* 2019 Element replacement approach by reaction with Lewis acidic molten salts to synthesize nanolaminated MAX phases and MXenes *J. Am. Chem. Soc.* **141** 4730–7
[131] Li Y *et al* 2020 A general Lewis acidic etching route for preparing MXenes with enhanced electrochemical performance in non-aqueous electrolyte *Nat. Mater.* **19** 894–9
[132] Dhamodharan D, Dhinakaran V and Byun H-S 2022 MXenes: an emerging 2D material *Carbon* **192** 366–83
[133] Li Y *et al* 2021 Author correction: a general Lewis acidic etching route for preparing MXenes with enhanced electrochemical performance in non-aqueous electrolyte *Nat. Mater.* **20** 571
[134] Wei Y *et al* 2021 Advances in the synthesis of 2D Mxenes *Adv. Mater.* **33** 2103148
[135] Shi H, Zhang P, Liu Z, Park S, Lohe M R, Wu Y, Shaygan Nia A, Yang S and Feng X 2021 Ambient-stable two-dimensional titanium carbide (MXene) Enabled by iodine etching *Angew. Chem., Int. Ed. Engl.* **60** 8689–93
[136] Jawaid A, Hassan A, Neher G, Nepal D, Pachter R, Kennedy W J, Ramakrishnan S and Vaia R A 2021 Halogen etch of Ti_3AlC_2 MAX phase for MXene fabrication *ACS Nano* **15** 2771–7
[137] Panda S *et al* 2022 MXene based emerging materials for supercapacitor applications: recent advances, challenges, and future perspectives *Coord. Chem. Rev.* **462** 214518
[138] Hadler-Jacobsen J *et al* 2021 Stacking sequence, interlayer bonding, termination group stability and Li/Na/Mg diffusion in MXenes *ACS Mater. Lett.* **3** 1369–76
[139] Hu T, Hu M, Li Z, Zhang H, Zhang C, Wang J and Wang X 2016 Interlayer coupling in two-dimensional titanium carbide MXenes *Phys. Chem. Chem. Phys.* **18** 20256–60
[140] Wu Y *et al* 2021 Recent advances in transition metal carbides and nitrides (MXenes): characteristics, environmental remediation and challenges *Chem. Eng. J.* **418** 129296
[141] Lai S, Jeon J, Jang S K, Xu J, Choi Y J, Park J-H, Hwang E and Lee S 2015 Surface group modification and carrier transport properties of layered transition metal carbides (Ti_2CT_x, T: –OH, –F and –O) *Nanoscale* **7** 19390–6
[142] Naguib M, Unocic R R, Armstrong B L and Nanda J 2015 Large-scale delamination of multi-layers transition metal carbides and carbonitrides "MXenes" *Dalton Trans.* **44** 9353–8
[143] Tao Q *et al* 2017 Two-dimensional Mo 1.33 C MXene with divacancy ordering prepared from parent 3D laminate with in-plane chemical ordering *Nat. Commun.* **8** 1–7
[144] Xu J *et al* 2021 Recent advances in 2D MXenes: preparation, intercalation and applications in flexible devices *J. Mater. Chem.* A **9** 14147–71
[145] Han F *et al* 2019 Boosting the yield of MXene 2D sheets via a facile hydrothermal-assisted intercalation *ACS Appl. Mater. Interfaces* **11** 8443–52
[146] Wu W *et al* 2018 Two-dimensional nanosheets by rapid and efficient microwave exfoliation of layered materials *Chem. Mater.* **30** 5932–40
[147] Natu V *et al* 2020 2D Ti_3C_2Tz MXene synthesized by water-free etching of Ti_3AlC_2 in polar organic solvents *Chem* **6** 616–30
[148] Xuan J *et al* 2016 Organic-base-driven intercalation and delamination for the production of functionalized titanium carbide nanosheets with superior photothermal therapeutic performance *Angew. Chem.* **128** 14789–94
[149] Fujishima A and Honda K 1972 Electrochemical photolysis of water at a semiconductor electrode *Nature* **238** 37e38
[150] Li X *et al* 2020 Principle and surface science of photocatalysis *Interface Sci. Technol.* **31** 1–38
[151] Liu B, Wu H and Parkin I P 2020 New insights into the fundamental principle of semiconductor photocatalysis *ACS Omega* **5** 14847–56
[152] Li K *et al* 2021 MXenes as noble-metal-alternative co-catalysts in photocatalysis *Chin. J. Catal.* **42** 3–14
[153] Zhuang Y, Liu Y and Meng X 2019 Fabrication of TiO_2 nanofibers/MXene Ti_3C_2 nanocomposites for photocatalytic H_2 evolution by electrostatic self-assembly *Appl. Surf. Sci.* **496** 143647
[154] Ye M, Wang X, Liu E, Ye J and Wang D 2018 Boosting the photocatalytic activity of P25 for carbon dioxide reduction by using a surface-alkalinized titanium carbide MXene as cocatalyst *ChemSusChem* **11** 1606–11

[155] Zhong Q, Li Y and Zhang G 2020 Two-dimensional MXene-based and MXene-derived photocatalysts: recent developments and perspectives *Chem. Eng. J.* **409** 128099
[156] Liu Z, Zhou Y, Yang L and Yang R 2021 Green preparation of *in-situ* oxidized TiO_2/Ti_3C_2 heterostructure for photocatalytic hydrogen production *Adv. Powder Technol.* **32** 4857–61
[157] Meili C, Jungbluth N and Annaheim J, 2018 Life cycle inventories of crude oil extraction ESU-services Ltd.commissioned by BAFU, BFE & Erdöl-Vereinigung Schaff-Hausen
[158] Bai S *et al* 2021 Recent advances of MXenes as electrocatalysts for hydrogen evolution reaction *npj 2D Mater. Appl.* **5** 1–15
[159] Wang M, Han K, Zhang S and Sun L 2015 Integration of organometallic complexes with semiconductors and other nanomaterials for photocatalytic H_2 production *Coord. Chem. Rev.* **287** 1–14
[160] Sherryna A and Tahir M 2021 Role of Ti_3C_2 MXene as prominent schottky barriers in driving hydrogen production through photoinduced water splitting: a comprehensive review *ACS Appl. Energy Mater.* **4** 11982–2006
[161] Ran J, Gao G, Li F-T, Ma T-Y, Du A and Qiao S-Z 2017 Ti_3C_2 MXene co-catalyst on metal sulfide photo-absorbers for enhanced visible-light photocatalytic hydrogen production *Nat. Commun.* **8** 1–10
[162] Nørskov J K, Bligaard T, Logadottir A, Kitchin J R, Chen J G, Pandelov S and Stimming U 2005 Trends in the exchange current for hydrogen evolution *J. Electrochem. Soc.* **152** J23
[163] Liu J, Zhang H-B, Sun R, Liu Y, Liu Z, Zhou A and Yu Z-Z 2017 Hydrophobic, flexible, and lightweight MXene foams for high-performance electromagnetic-interference shielding *Adv. Mater.* **29** 1702367
[164] Sreedhar A and Noh J-S 2021 Recent advances in partially and completely derived 2D Ti_3C_2 MXene based TiO_2 nanocomposites towards photocatalytic applications: a review *Sol. Energy* **222** 48–73
[165] Im J K, Sohn E J, Kim S, Jang M, Son A, Zoh K-D and Yoon Y 2020 Review of MXene-based nanocomposites for photocatalysis *Chemosphere* **270** 129478
[166] Qin X *et al* 2022 Hydrothermal growth of ZnCdS/TiO_2 nanoparticles on the surface of the Ti_3C_2 MXene sheet to enhance photocatalytic performance under visible light *J. Solid State Chem.* **306** 122750
[167] Nguyen V-H *et al* 2020 Novel architecture titanium carbide ($Ti_3C_2T_x$) MXene cocatalysts toward photocatalytic hydrogen production: a mini-review *Nanomaterials* **10** 602
[168] Xiao R, Zhao C, Zou Z, Chen Z, Tian L, Xu H, Tang H, Liu Q, Lin Z and Yang X 2020 *In situ* fabrication of 1D CdS nanorod/2D Ti_3C_2 MXene nanosheet Schottky heterojunction toward enhanced photocatalytic hydrogen evolution *Appl. Catal.* B **268** 118382
[169] Yang W, Ma G, Fu Y, Peng K, Yang H, Zhan X, Yang W, Wang L and Hou H 2022 Rationally designed Ti_3C_2 MXene@ $TiO_2/CuInS_2$ Schottky/S-scheme integrated heterojunction for enhanced photocatalytic hydrogen evolution *Chem. Eng. J.* **429** 132381
[170] Xie G, Zhu Y, Yu C, Xie X and Zhang N 2023 Engineered charge transfer and reactive site over hierarchical Ti_3C_2Tx MXene@In_2S_3-NiS toward enhanced photocatalytic H_2 evolution *2D Mater.* **10** 014004
[171] Huang K, Li C, Zhang X, Wang L, Wang W and Meng X 2021 Self-assembly synthesis of phosphorus-doped tubular g-C_3N_4/Ti_3C_2 MXene Schottky junction for boosting photocatalytic hydrogen evolution *Green Energy Environ.* accepted (https://doi.org/10.1016/j.gee.2021.03.011)
[172] Cao B, Wan S, Wang Y, Guo H, Ou M and Zhong Q 2022 Highly-efficient visible-light-driven photocatalytic H_2 evolution integrated with microplastic degradation over MXene/ZnxCd$_1$-xS photocatalyst *J. Colloid Interface Sci.* **605** 311–9
[173] Li X, Bai Y, Shi X, Huang J, Zhang K, Wang R and Ye L 2021 Mesoporous g-C_3N_4/MXene ($Ti_3C_2T_x$) heterojunction as a 2D electronic charge transfer for efficient photocatalytic CO_2 reduction *Appl. Surf. Sci.* **546** 149111
[174] Zeng G, Cao Y, Wu Y, Yuan H, Zhang B, Wang Y, Zeng H and Huang S 2021 Cd0. 5Zn0. 5S/Ti_3C_2 MXene as a Schottky catalyst for highly efficient photocatalytic hydrogen evolution in seawater *Appl. Mater. Today* **22** 100926
[175] Huang K, Li C and Meng X 2020 *In-situ* construction of ternary Ti_3C_2 MXene@ $TiO_2/ZnIn_2S_4$ composites for highly efficient photocatalytic hydrogen evolution *J. Colloid Interface Sci.* **580** 669–80
[176] Yang J-X *et al* 2021 PtO nanodots promoting Ti_3C_2 MXene *in-situ* converted Ti_3C_2/TiO_2 composites for photocatalytic hydrogen production *J. Chem. Eng.* **420** 129695
[177] Huang J *et al* 2022 *In situ* construction of 1D CdS/2D Nb_2CTx MXene Schottky heterojunction for enhanced photocatalytic hydrogen production activity *Appl. Surf. Sci.* **573** 151491
[178] Ou M *et al* 2021 Formation of noble-metal-free 2D/2D $ZnmIn_2Sm+$ 3 (m= 1, 2, 3)/MXene Schottky heterojunction as an efficient photocatalyst for hydrogen evolution *Chem. Eng. J.* **424** 130170
[179] Li J, Li J, Wu C, Li Z, Cai L, Tang H and Wang S 2021 Crystalline carbon nitride anchored on MXene as an ordered Schottky heterojunction photocatalyst for enhanced visible-light hydrogen evolution *Carbon* **179** 387–99
[180] Wang H *et al* 2021 Ti_3C_2 Mxene modified $SnNb_2O_6$ nanosheets Schottky photocatalysts with directed internal electric field for tetracycline hydrochloride removal and hydrogen evolution *Sep. Purif. Technol.* **265** 118516
[181] Zheng S *et al* 2021 Schottky-structured 0D/2D composites via electrostatic self-assembly for efficient photocatalytic hydrogen evolution *Ceram. Int.* **47** 28304–11
[182] Song T, Hou L, Long B, Ali A and Deng G-J 2021 Ultrathin MXene "bridge" to accelerate charge transfer in ultrathin metal-free 0D/2D black phosphorus/g-C_3N_4 heterojunction toward photocatalytic hydrogen production *J. Colloid Interface Sci.* **584** 474–83
[183] Kang J *et al* 2020 Design of three-dimensional hollow-sphere architecture of $Ti_3C_2T_x$ MXene with graphitic carbon nitride nanoshells for efficient photocatalytic hydrogen evolution *ACS Appl. Energy Mater.* **3** 9226–33
[184] Han X *et al* 2020 Ti_3C_2 MXene-derived carbon-doped TiO_2 coupled with g-C_3N_4 as the visible-light photocatalysts for photocatalytic H_2 generation *Appl. Catal.* B **265** 118539
[185] Xu H *et al* 2021 *In situ* construction of protonated g-C_3N_4/Ti_3C2 MXene Schottky heterojunctions for efficient photocatalytic hydrogen production *Chin. J. Catal.* **42** 107–14
[186] Su T, Hood Z D, Naguib M, Bai L, Luo S, Rouleau C M, Ivanov I N, Ji H, Qin Z and Wu Z 2019 2D/2D heterojunction of Ti_3C_2/gC_3N_4 nanosheets for enhanced photocatalytic hydrogen evolution *Nanoscale* **11** 8138–49
[187] Wang K *et al* 2021 *In situ* grown monolayer N–doped graphene and ZnO on $ZnFe_2O_4$ hollow spheres for efficient photocatalytic tetracycline degradation *Colloids Surf.* A **618** 126362
[188] Bie C *et al* 2019 *In situ* grown monolayer N-doped graphene on CdS hollow spheres with seamless contact for photocatalytic CO_2 reduction *Adv. Mater.* **31** 1902868
[189] Song X *et al* 2020 Fabricating C and O co-doped carbon nitride with intramolecular donor-acceptor systems for efficient photoreduction of CO_2 to CO *Appl. Catal.* B **268** 118736
[190] Li J *et al* 2021 Van der Waals heterojunction for selective visible-light-driven photocatalytic CO_2 reduction *Appl. Catal.* B **284** 119733
[191] Ghoreishian S M *et al* 2021 Full-spectrum-responsive Bi_2S_3@ CdS S-scheme heterostructure with intimated

ultrathin RGO toward photocatalytic Cr (VI) reduction and H_2O_2 production: experimental and DFT studies *Chem. Eng. J.* **419** 129530
[192] Hu J, Ding J and Zhong Q 2021 Ultrathin 2D Ti_3C_2 MXene Co-catalyst anchored on porous g-C_3N_4 for enhanced photocatalytic CO_2 reduction under visible-light irradiation *J. Colloid Interface Sci.* **582** 647–57
[193] Sreedhar A, Reddy I N and Noh J S 2021 Photocatalytic and electrocatalytic reduction of CO_2 and N_2 by Ti_3C_2 MXene supported composites for a cleaner environment: a review *J. Clean. Prod.* **328** 129647
[194] Shen J *et al* 2021 Emerging applications of MXene materials in CO_2 photocatalysis *Flatchem* **28** 100252
[195] Fu J *et al* 2020 Product selectivity of photocatalytic CO_2 reduction reactions *Mater. Today* **32** 222–43
[196] Li K, Peng B and Peng T 2016 Recent advances in heterogeneous photocatalytic CO_2 conversion to solar fuels *ACS Catal.* **6** 7485–527
[197] White J L *et al* 2015 Light-driven heterogeneous reduction of carbon dioxide: photocatalysts and photoelectrodes *Chem. Rev.* **115** 12888–935
[198] Li J, Wang Z, Chen H, Zhang Q, Hu H, Liu L, Ye J and Wang D 2021 A surface-alkalinized Ti_3C_2 MXene as an efficient cocatalyst for enhanced photocatalytic CO_2 reduction over ZnO *Catal. Sci. Technol.* **11** 4953–61
[199] Tahir M and Tahir B 2021 *In-situ* growth of TiO_2 imbedded Ti_3C_2TA nanosheets to construct PCN/Ti_3C_2TA MXenes 2D/3D heterojunction for efficient solar driven photocatalytic CO_2 reduction towards CO and CH_4 production *J. Colloid Interface Sci.* **591** 20–37
[200] Low J, Suzuki R, Krüger T, Frey E and Bausch A R 2018 TiO_2/MXene Ti_3C_2 composite with excellent photocatalytic CO_2 reduction activity *J. Catal.* **361** 255–66
[201] Saeed A *et al* 2021 Enhancement of photocatalytic CO_2 reduction for novel Cd0. 2Zn0. 8S@ Ti_3C_2 (MXenes) nanocomposites *J. CO2 Util.* **47** 101501
[202] Khan A A, Tahir M and Zakaria Z Y 2021 Synergistic effect of anatase/rutile TiO_2 with exfoliated Ti_3C_2TR MXene multilayers composite for enhanced CO_2 photoreduction via dry and bi-reforming of methane under UV–visible light *J. Environ. Chem. Eng.* **9** 105244
[203] Chen Y-H *et al* 2021 Activating two-dimensional Ti_3C_2Tx-MXene with single-atom cobalt for efficient CO_2 photoreduction *Cell Rep. Phys. Sci.* **2** 100371
[204] He F *et al* 2020 2D/2D/0D TiO_2/C_3N_4/Ti_3C_2 MXene composite S-scheme photocatalyst with enhanced CO_2 reduction activity *Appl. Catal.* B **272** 119006
[205] Yang C *et al* 2020 2D/2D Ti_3C_2 MXene/g-C_3N_4 nanosheets heterojunction for high efficient CO_2 reduction photocatalyst: dual effects of urea *Appl. Catal.* B **268** 118738
[206] Tang Q, Sun Z, Deng S, Wang H and Wu Z 2020 Decorating g-C_3N_4 with alkalinized Ti_3C_2 MXene for promoted photocatalytic CO_2 reduction performance *J. Colloid Interface Sci.* **564** 406–17
[207] Chen W *et al* 2020 Ultrathin Co-Co LDHs nanosheets assembled vertically on MXene: 3D nanoarrays for boosted visible-light-driven CO_2 reduction *Chem. Eng. J.* **391** 123519
[208] Zhang J *et al* 2021 Cu_2O/Ti_3C_2MXene heterojunction photocatalysts for improved CO_2 photocatalytic reduction performance *Appl. Surf. Sci.* **542** 148685
[209] Fang Y, Cao Y, Tan B and Chen Q 2021 Oxygen and titanium vacancies in a BiOBr/MXene-Ti_3C_2 composite for boosting photocatalytic N_2 fixation *ACS Appl. Mater. Interfaces* **13** 42624–34
[210] Chang B, Guo Y, Wu D, Li L, Yang B and Wang J 2021 Plasmon-enabled N_2 photofixation on partially reduced Ti_3C_2 MXene *Chem. Sci.* **12** 11213–24
[211] Hao C *et al* 2020 RuO_2-loaded TiO_2–MXene as a high performance photocatalyst for nitrogen fixation *J. Phys. Chem. Solids* **136** 109141
[212] Chen X, Li Y, Wu Z, Xu X, Zhu W and Gao X 2021 $Bi_4O_5Br_2$ anchored on Ti_3C_2 MXene with ohmic heterojunction in photocatalytic NH_3 production: insights from combined experimental and theoretical calculations *J. Colloid Interface Sci.* **602** 553–62
[213] Jiang H *et al* 2020 2D MXene-derived Nb_2O_5/C/Nb_2C/gC_3N_4 heterojunctions for efficient nitrogen photofixation *Catal. Sci. Technol.* **10** 5964–72
[214] Gao W, Li X, Luo S, Luo Z, Zhang X, Huang R and Luo M 2021 *In situ* modification of cobalt on MXene/TiO_2 as composite photocatalyst for efficient nitrogen fixation *J. Colloid Interface Sci.* **585** 20–29
[215] Sun B *et al* 2021 The fabrication of 1D/2D CdS nanorod@ Ti_3C_2 MXene composites for good photocatalytic activity of hydrogen generation and ammonia synthesis *Chem. Eng. J.* **406** 127177
[216] Hou T *et al* 2020 Near-infrared light-driven photofixation of nitrogen over Ti_3C_2Tx/TiO_2 hybrid structures with superior activity and stability *Appl. Catal.* B **273** 119072
[217] Liu Q, Ai L and Jiang J 2018 MXene-derived TiO_2@ C/gC_3N_4 heterojunctions for highly efficient nitrogen photofixation *J. Mater. Chem.* A **6** 4102–10
[218] Qin X *et al* 2021 Hydrothermal growth of ZnCdS/TiO_2 nanoparticles on the surface of the Ti_3C_2 MXene sheet to enhance photocatalytic performance under visible light *J. Solid State Chem.* 122750
[219] Zou X, Zhao X, Zhang J, Lv W, Qiu L and Zhang Z 2021 Photocatalytic degradation of ranitidine and reduction of nitrosamine dimethylamine formation potential over MXene–Ti_3C_2/MoS_2 under visible light irradiation *J. Hazard. Mater.* **413** 125424
[220] Fang Y, Cao Y and Chen Q 2019 Synthesis of an Ag_2WO_4/Ti_3C_2 Schottky composite by electrostatic traction and its photocatalytic activity *Ceram. Int.* **45** 22298–307
[221] Jiang X *et al* 2020 Two-dimensional MXenes: from morphological to optical, electric, and magnetic properties and applications *Phys. Rep.* **848** 1–58
[222] Khan R and Andreescu S J S 2020 Mxenes-based bioanalytical sensors: design, characterization, and applications *Sensors* **20** 5434
[223] Dong L M *et al* 2020 Two-dimensional metal carbides and nitrides (MXenes): preparation, property, and applications in cancer therapy *Nanophotonics* **9** 2125–45
[224] Iqbal M Z and Siddique S 2021 Two-dimensional transition metal carbides and nitrides (MXenes): synthesis to applications *Contemporary Nanomaterials in Material Engineering Applications* (Berlin: Springer) pp 179–99
[225] Shahzad A, Jang J, Lim S-R and Lee D S 2020 Unique selectivity and rapid uptake of molybdenum-disulfide-functionalized MXene nanocomposite for mercury adsorption *Environ. Res.* **182** 109005
[226] Shahzad A *et al* 2019 $Ti_3C_2T_x$ MXene core-shell spheres for ultrahigh removal of mercuric ions *Chem. Eng. J.* **368** 400–8
[227] Berkani M, Smaali A, Almomani F and Vasseghian Y 2021 Recent advances in MXene-based nanomaterials for desalination at water interfaces *Environ. Res.* **203** 111845
[228] Feng X *et al* 2021 3D MXene/Ag_2S material as Schottky junction catalyst with stable and enhanced photocatalytic activity and photocorrosion resistance *Sep. Purif. Technol.* **266** 118606
[229] Su T *et al* 2019 Monolayer $Ti_3C_2T_x$ as an effective co-catalyst for enhanced photocatalytic hydrogen production over TiO_2 *ACS Appl. Energy Mater.* **2** 4640–51
[230] Iqbal A *et al* 2021 Improving oxidation stability of 2D MXenes: synthesis, storage media, and conditions *Nano Converg.* **8** 1–22
[231] Thirumal V, Yuvakkumar R, Kumar P S, Keerthana S P, Ravi G, Velauthapillai D and Saravanakumar B 2021 Efficient photocatalytic degradation of hazardous pollutants by homemade kitchen blender novel technique via 2D-material of few-layer MXene nanosheets *Chemosphere* **281** 130984

[232] Miao Z, Wang G, Zhang X and Dong X 2020 Oxygen vacancies modified TiO_2/Ti_3C_2 derived from MXenes for enhanced photocatalytic degradation of organic pollutants: the crucial role of oxygen vacancy to schottky junction *Appl. Surf. Sci.* **528** 146929
[233] Long R, Yu Z, Tan Q, Feng X, Zhu X, Li X and Wang P 2021 Ti_3C_2 MXene/NH_2-MIL-88B (Fe): research on the adsorption kinetics and photocatalytic performance of an efficient integrated photocatalytic adsorbent *Appl. Surf. Sci.* **570** 151244
[234] Guo S *et al* 2021 Construction of hierarchical $Ti_3C_2T_x$ MXene/$ZnIn_2S_4$ heterostructures for efficiently photocatalytic reduction of Cr (VI) under visible light *Appl. Surf. Sci.* **575** 151753
[235] Khadidja M F *et al* 2021 Hierarchical ZnO/MXene composites and their photocatalytic performances *Colloids Surf.* A **628** 127230
[236] Quyen V T, Ha L T T, Thanh D M, Le Q V, Viet N M, Nham N T and Thang P Q 2021 Advanced synthesis of MXene-derived nanoflower-shaped TiO_2@ Ti_3C_2 heterojunction to enhance photocatalytic degradation of Rhodamine B *Environ. Technol. Innov.* **21** 101286
[237] Huang K *et al* 2021 Layered Ti_3C_2 MXene and silver co-modified g-C_3N_4 with enhanced visible light-driven photocatalytic activity *Chem. Eng. J.* **425** 131493
[238] Alsafari I A *et al* 2021 Synthesis, characterization, photocatalytic and antibacterial properties of copper Ferrite/MXene ($CuFe_2O_4/Ti_3C_2$) nanohybrids *Ceram. Int.* **47** 28874–83
[239] Song H, Wang Y, Ling Z, Zu D, Li Z, Shen Y and Li C 2020 Enhanced photocatalytic degradation of perfluorooctanoic acid by Ti_3C_2 MXene-derived heterojunction photocatalyst: application of intercalation strategy in DESs *Sci. Total Environ.* **746** 141009